Data Driven Modeling and Optimization of MEA Absorption Process for CO_2 Capture

by

Abdelhamid Shalaby

A thesis
presented to the University of Waterloo
in fulfilment of the
thesis requirement for the degree of
Master of Applied Science
in
Chemical Engineering

Waterloo, Ontario, Canada, 2020

AUTHOR'S DECLARATION

I hereby declare that I am the sole author of this thesis. This is a true copy of the thesis, including any required final revisions, as accepted by my examiners.

I understand that my thesis may be made electronically available to the public.

Abstract

Global warming is a rising issue and there are many research studies aiming to reduce the greenhouse gas emissions. Carbon capture and storage technologies improved throughout the years to contribute as a solution to this problem. In this work the post combustion carbon capture unit is used to develop surrogated models for operation optimization.

Previous work included mechanistic and detailed modelling of steady state and dynamic systems. Furthermore, control structures and optimization approaches have been studied. Moreover, various solutions such as *MEA*, *DEA* and *MDEA* have been tested and simulated to determine the efficiency and the behaviour of the system. In this work a dynamic model with *MEA* solution developed by (Nittaya, 2014) and (Harun, 2012) is used to generate operation data. The system is simulated using gProms v.5.1 with six PI controllers. The model illustrated that the regeneration of the solvent is the most energy consuming part of the process. Due to the changes of electricity supply and demand, also, the importance of achieving a specific *%CC* and purity of carbon dioxide as outputs of this process, surrogated models are developed and used to predict the outputs and to optimize the operating conditions of the process.

Multiple machine learning and data driven models has been developed using simulation data generated after a proper choice of the operating variables and the important outputs. Steady state and transient state models have been developed and evaluated. The models were used to predict the outputs of the process and used later to optimize the operating conditions of the process. The flue gas flow rate, temperature, pressure, reboiler pressure, reboiler and condenser duties were selected as the operating variables of the system (inputs). The system energy requirements, *%CC* and the purity of carbon dioxide were selected to be the outputs of the process. For steady state modelling, artificial neural network (*ANN*) model with backpropagation and momentum was developed to predict the process outputs. The *ANN* model efficiency was compared to other machine learning models such as Gaussian Process Regression (*GPR*), rational quadratic *GPR*, squared exponential *GPR*, tree regression and matern *GPR*. The *ANN* excelled all other models in terms of prediction and accuracy, however, the other model's regression coefficient (R^2) was never below 0.95.

For dynamic modelling, recurrent neural networks (*RNN*) have been used to predict the outputs of the system. Two training algorithms have been used to create the neural network: Levenberg-Marquardt (*LM*) and Broyden-Fletcher-Goldfrab-Shanno (*BFGS*). The *RNN* was able to predict the outputs of the system accurately. Sequential quadratic programming (*SQP*) and genetic algorithm (*GA*) were used to optimize the surrogated models and determine the optimum operating conditions following an objective of maximizing the purity of CO_2 and *%CC* and minimizing the system energy requirements.

Acknowledgements

First and foremost, praises to Allah for providing me the power and ability to conduct and complete my research successfully. I would like to express my deepest gratitude to Professor Peter Douglas and Ali Elkamel my supervisors, for believing in me and providing me the opportunity with full guidance through research.

I am extremely grateful to my parents and specially my mom Mona Alrami, whom the reason why I became an engineer. A special thanks to my father, Mohammed Shalaby and my amazing and supporting big brother Mahmoud Shalaby, my beautiful sister, and my role model Dr. Nouran Shalaby, my future engineer brother Yousef Shalaby. A special thanks to my best friend engineer Sameh Zawawi for his continuous support. I am very thankful to my friends and everyone for their love and prayers to have a successful career.

Dedication

Dedicated to my beloved parents

Table of Contents

List of Figures

List of Tables

Chapter 1: Introduction

The rise in concern for climate change and global warming motivated the research to advance in reducing the greenhouse gases emissions specifically carbon dioxide. Since the industrial revelation in the eighteenth century, humankind dependency on fossil fuels as a source of energy has increased, leading to fast growth in technology and lifestyle developments. Unfortunately, the awareness of the environmental effects due to the growth of industry and transportation emissions, risen after the clear vision of the global warming (Jacobson, 2009).

One great problem developed is the greenhouse gas effect, where the gases in the upper atmosphere absorb the heat and radiations from the earth's surface and reflect them back. The greenhouse gases are carbon dioxide (CO_2), methane (CH_4) and nitrous oxide. (N_2O) These gases results in the increase of the earth's surface temperature and affects the ecological and environmental system. As the production of electricity is the major contributor for carbon dioxide emissions, many countries attempt to shift towards renewable sources such as solar, hydro and wind to produce electricity (Ranisau et al., 2017). Carbon capture and storage (*CCS*) technologies can be viewed as a solution to reduce the emissions from an existing fossil fuels power plant.

Three main types of *CCS* methods are pre-combustion, oxyfuel and post-combustion. For the pre-combustion and oxyfuel, one must keep in mind that these technologies must be included during the design phase of a plant. On the other hand, post-combustion became a mature and reliable solution due to the extensive research done on it and the fact of it being retrofitted on existing power plants. Steady state models were developed to have a better understanding of the system and its capabilities, and the changes due to the change of the operating conditions. Experiments on lab-scale plants were necessary to observe the effect of using different solvents and to develop dynamic and more mechanistic models (Ahmad, 2019).

A better understanding of the operating conditions and the variables that affects the process is required to perform optimization. Optimizing the operating conditions of the process leads to saving cost while maintaining desirable outputs of the process. Investigations of operating conditions such as the flow rate of flue gas, solvent type, and controller designs

1.1 Thesis Outline

The objective of this research is to develop surrogated models using machine learning techniques to simulate the process. The models used to predict the outputs of both steady state and dynamic systems. Moreover, this research illustrates the possibilities of performing optimization over the surrogated models to obtain the optimal operating conditions for the process.

Chapter 2 includes the literature review where previous work and background of the process modelling is presented. An overview of the *CCS* is discussed in detail to provide the understanding of different systems.

Chapter 3 illustrates the post-combustion system used in this work and describe the capturing process. Sensitivity analysis, steady state, dynamic modelling is explained, and the results are discussed.

Chapter 4 presents the optimization over the developed models and discuss the key findings results. While the last chapter is conclusion and recommendation for future work is provided.

Chapter 2: Literature Review

2.1 Background

Global warming has been a rising issue for the past two decades, and it is our duty as human beings and the main cause of climate change to act fast to solve this problem. The rising in Earth's surface temperature is affecting the ecological system and causing many problems such as desertification, melting of snow and ice, sea level rise and weather changes around the globe (Draper & Weissburg, 2019). Greenhouse effect occurring naturally maintains Earth's temperature at a level making life possible for all organisms, however, since the industrial revolution human started contributing in increasing the greenhouse effect due to the gas emissions proved by many scientific research studies with more than 90% certainty (Hansen, Ruedy, Sato, & Lo, 2010).

The climate change is illustrated by the fact of accelerated melting of ice and glaciers which causes the rise in sea level. It is also noticed the change in weather patterns as some places became dryer and other places became wetter with stronger storms and floods. Humans' industrial activities caused the rise in carbon dioxide (CO_2), nitrogen oxides (NO_x) and methane (CH_4) gases in the atmosphere named greenhouse gases (*GHG*) (Ahmad, 2019). These gases prevent the transmitted heat and light from the Earth's surface to escape the atmosphere. Furthermore, the *GHG* reflect this heat and light back to the surface causing the rise in the temperature.

Burning fossil fuels such as coal and oil as a source of energy, and oil refineries are the main source of carbon dioxide emissions (Jacobson, 2009). Methane is created due to the production and use of fossil fuels, livestock and rice farming and landfills. On the other hand, nitrogen oxides emissions are caused by synthetic fertilizers for agricultural purposes and combustion of human machinery. Another class of gases which are the fluorinated gases, contributes to the greenhouse effect because of being used in refrigeration processes and cooling applications.

Deforestation is one major problem caused by humans and it increase the global warming issue.

Changing many forests into farms or cutting trees for wood use or as a source of fuel has a huge impact on climate change. The absorption of carbon dioxide naturally by the trees decreases and the wind shield effect by the forests is eliminated. Furthermore, the rate of decomposition and soil disturbance increase, and this increase the carbon dioxide emissions (Jacobson, 2009).

There are four major consequences of global warming and climate change, desertification, melting of ice, sea level rising and weather changes across the world. Desertification is an issue rising from the increase of the earth's temperature making arid areas drier even than before. A lot of research studies showed that the water cycle is changing, and rain patterns are alternating to make dry area drier. Over 2.5 million people in the dry areas are suffering from shortages of water and an intense amount of distress (Jacobson, 2009).

Observing the Earth's poles where ice is the dominating element started to melt down due to climate change, also in the Alps, Himalayas and Alaska is serious (Jacobson, 2009). The perennial ice that covers the Arctic is melting at a rate of 12% per decade, and the thickness of the Arctic has decreased by almost 50% since 1960. Since 2002, the continent of Antarctica lost more 100 cubic kilometres of ice per year, this rate has doubled since 2010.

The ice melting is followed by an expected rise in the sea level. Since 1880, the sea level increased by 21 cm and the rising rate is accelerating. Oceans are expanding as well as the rise in temperature causes water expansion. Finally, stronger storms and hurricanes are observed since 1970 due to the rise in oceans' temperature. The Power Dissipation Index measures the destructive power of cyclones and hurricanes. *PDI* increased in the Pacific Ocean by 35% and has nearly doubled for the Atlantic. This tremendous change in weather behaviour can be simplified and explained as for every 1 ℃ increase in the water temperature increases the global frequency of category 4 and 5 storms by 31% (Jacobson, 2009).

There are many solutions proposed to overcome the global warming and climate change issue such as using alternative source of fuels such as biofuels and using renewable sources of energy that does not contribute in *GHGs* emissions. The renewable sources include solar photovoltaics, concentrated solar power, wind, hydroelectric and nuclear. First, solar photovoltaic (*PV*) are devices that converts solar radiations into a direct current. These devices compose of array of cells made of silicon base materials such as polycrystalline silicon or amorphous silicon where they are doped to increase the number of positive or negative charge carriers. The generation of electricity occurs when the positive and negative junctions are formed and illuminated. One major disadvantage of solar *PV* is that their efficiency decreases when the cells temperature exceeds 45 ℃ (Jacobson, 2009).

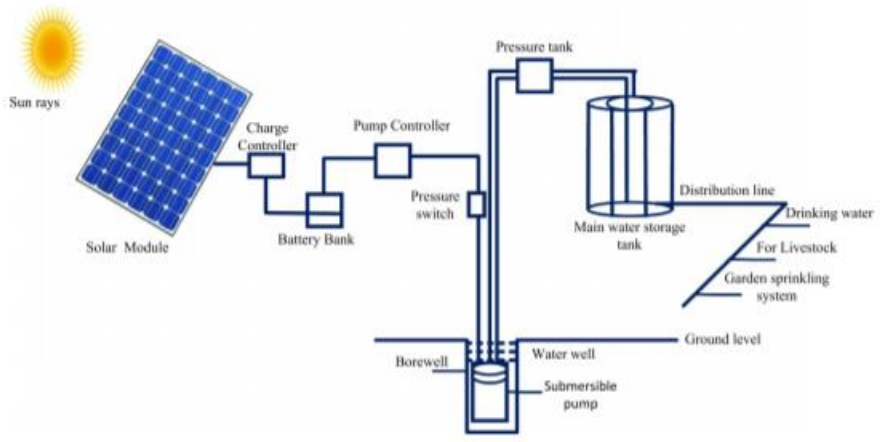

Figure 1: Solar photovoltaic diagram. (Poompavai & Kowsalya, 2019)

Secondly, concentrated solar power (*CSP*) is another technology that depends on the sunlight. Mirrors or reflective lenses reflects and concentrate sunlight and heat a fluid which flows to a heat engine to be converted to electricity. This fluid can be pressurized steam or synthetic oil or molten salts and located in a fluid collector at a high temperature. The collector can be a set parabolic mirrors that focuses light through a pipe containing the fluid to be heated then flowing to the chamber to heat water for steam generator and produces electricity. The other type of collectors can be a tower centred with set of reflectors surrounding the tower. The main

advantage of *CSP* that no cooling water is required as the power conversion unit is air cooled (Jacobson, 2009).

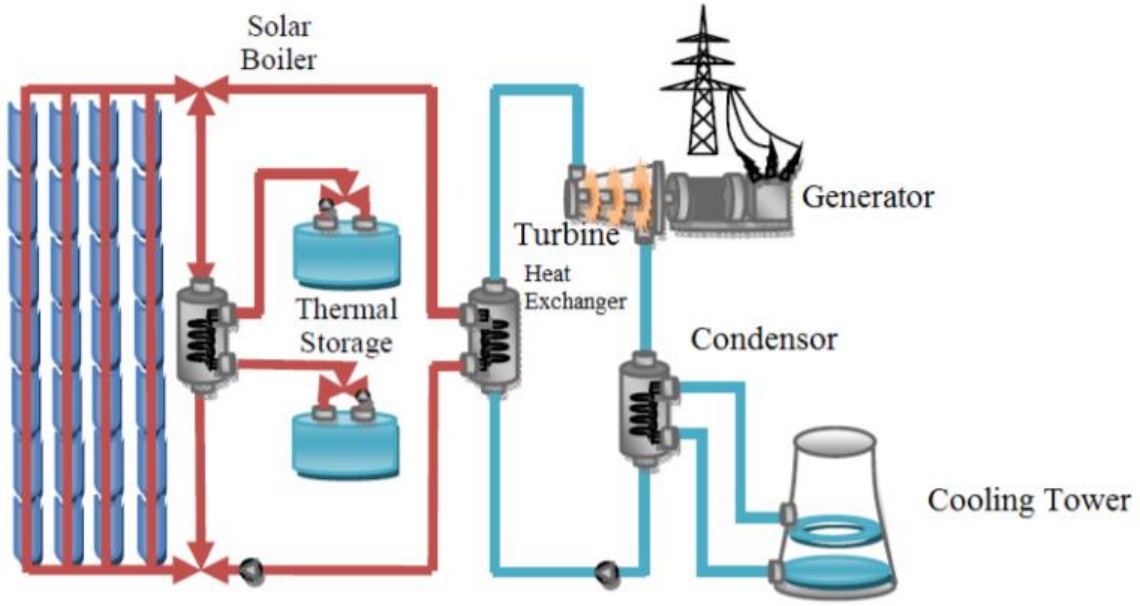

Figure 2: Concentrated solar power plant diagram. (Bishoyi & Sudhakar, 2017)

The third clean technology is wind turbines which converts the kinetic energy into electricity. This is done by converting the mechanical movements of a slow turning rotor inside a gearbox into fast rotating movements. The efficiency of wind turbines increases as the wind speed increases; hence, wind turbines are constructed on flat open areas and very high to capture and harness the maximum amount of kinetic energy. However, the speed and frequency of wind distribution are the major factors for wind turbines which makes them a non-reliable solution for some areas (Jacobson, 2009).

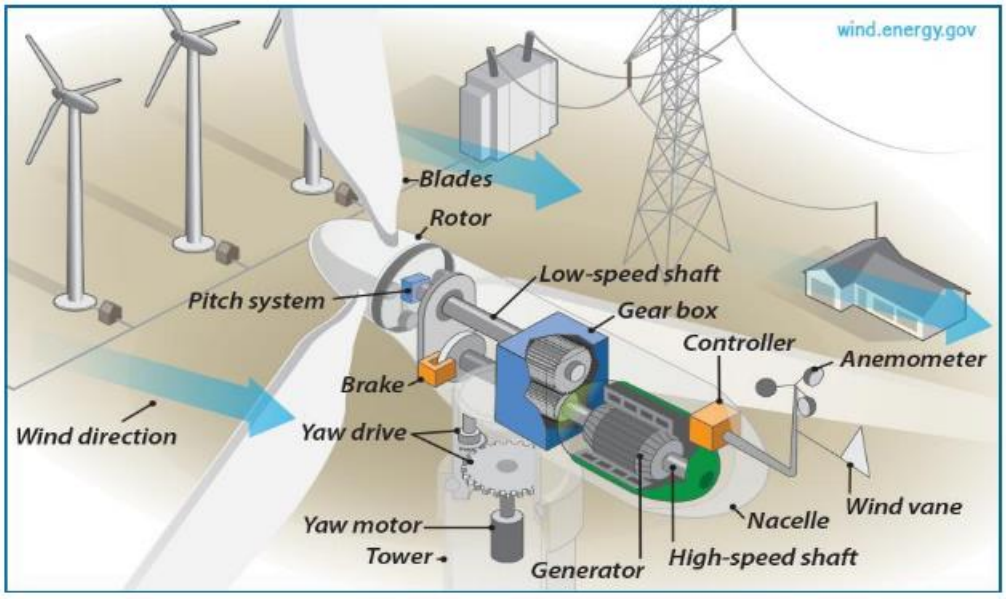

Figure 3: Wind turbine components. (Saifullah, Karim, & Karim, 2016)

Currently, hydroelectric power is the largest source of renewable power installed worldwide producing electricity. Electrical power is generated when water drops due to gravity driving turbines and generators. Dams are installed to collect water allowing the water falling through holes when needed. Nuclear power plants are also widely used as an alternative source of electricity generation. In nuclear plants the splitting of heavy elements such uranium during fission reaction, releases a huge amount of thermal energy that is used to generate steam to flow through turbines and generators to produce clean energy (Jacobson, 2009).

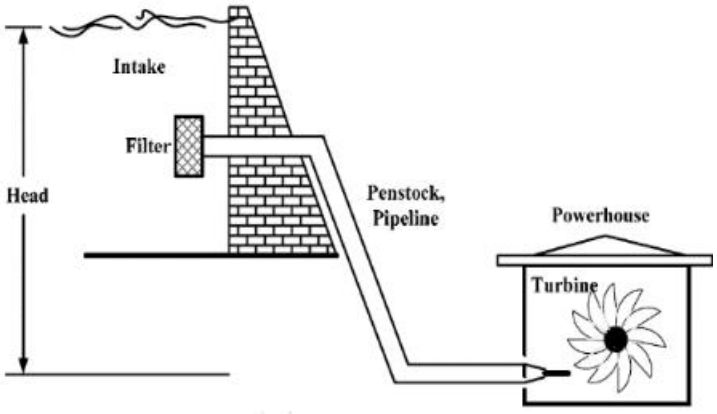

Figure 4: Hydroelectric power diagram.(Elbatran, Yaakob, Ahmed, & Ismail, 2015)

Furthermore, carbon capture and storage (*CCS*) is a solution to reduce the emissions specifically carbon dioxide (CO_2). In *CCS*, CO_2 is collected from point emission source and stored underground for other applications such as enhanced oil recovery (*EOR*)(Raza, Gholami, Rezaee, Rasouli, & Rabiei, 2019). There are three main technologies when it comes to carbon capture: pre-combustion, oxy-fuel and post combustion capturing. A detailed review on *CCS* technology is provided next chapter.

2.2 Pre-combustion Carbon Capture

In pre-combustion carbon capture, fossil fuels are converted into combustible gases used in for power generation. Carbon dioxide is separated from these gases before combustion. First, reforming or partial oxidation processes are used to produce synthesis gas (*syngas*). In reforming, hydrogen (H_2) and carbon monoxide (*CO*) are formed by adding high pressure steam to methane gas (CH_4)(Sifat & Haseli, 2019). Other reforming processes such as dry reforming of methane is used to produce syngas using catalyst instead of steam. On the other hand, in partial oxidation pure oxygen is supplied after being separated from air to the methane gas to produce syngas. Then, water-gas shift reaction is used to convert syngas to CO_2 (Sifat & Haseli, 2019).

Steam reforming: $CH_4 + H_2O \rightarrow CO + 3H_2$ (1)

Partial Oxidation: $CH_4 + 1/2\ O_2 \rightarrow CO + 2H_2$ (2)

Water-gas shift: $CO + H_2O \rightleftarrows CO_2 + H_2$ (3)

The CO_2 is removed easily at ambient temperature due to the high pressure from the water-gas shift reaction. The remaining gases (mainly hydrogen) are used to generate power. However, the energy requirement is high in the overall process due to the energy demand for separating oxygen from air in partial oxidation or steam requirement for reforming. An alternative to over sorption enhanced water-gas shift reaction (*SEWGS*) is used to increase the conversion of *CO* by removing carbon dioxide immediately from the products of the reaction (Sifat & Haseli, 2019). Many research studies proposed an integrated gasification combined cycle (*IGCC*) power plant to reduce the emissions. In *IGCC*, first oxygen is separated from air using pressure swing adsorption or any cryogenic air separation process. Then oxygen is blown to a gasifier where fossil fuel such as coal for example, is gasified under high pressure and temperature to produce syngas. Then syngas is cooled and treated to remove all impurities before converted to *CO* and CO_2 and H_2S. Cleaning and removal of sulphur compounds and other impurities is required after the water-gas shift process. The remaining products are H_2 and CO_2, and hydrogen is used then to produce power after the separation of CO_2.

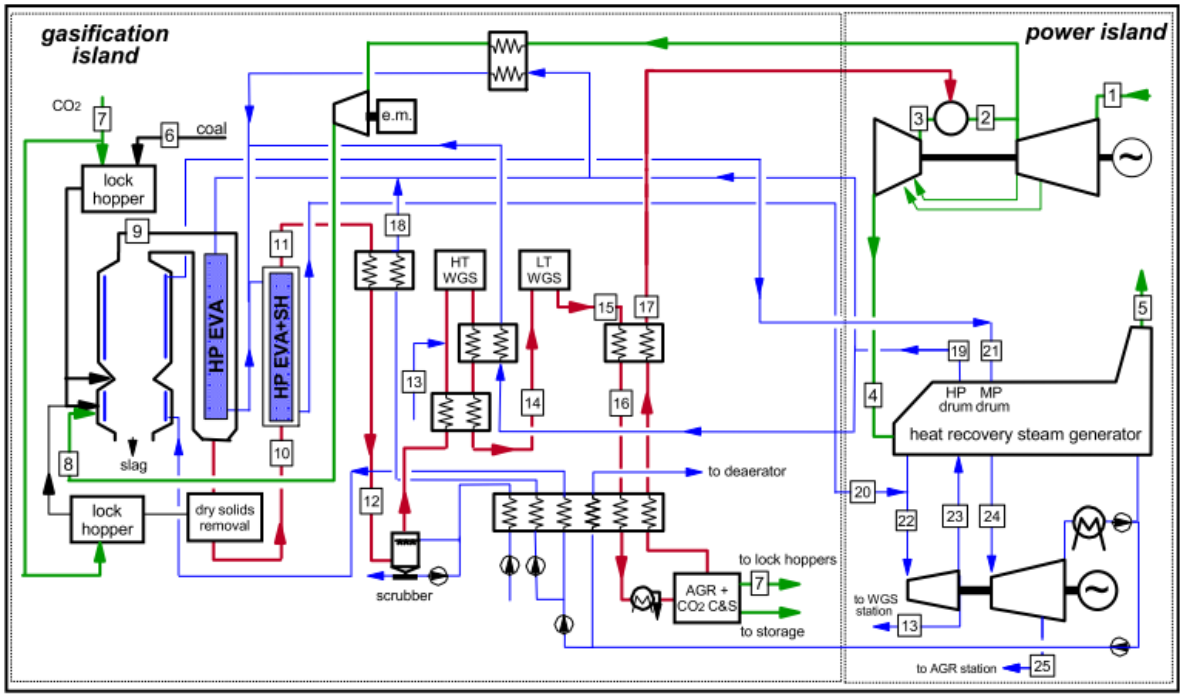

Figure 5: IGCC power plant with a pre-combustion capturing unit.(Moioli et al., 2014)

A lot of work has been done on the separation techniques of the pre-combustion capturing process. In 2010, (Romano, Chiesa, & Lozza, 2010) discussed the capturing of CO_2 using methyl di-ethanol amine (MDA) in absorption column and compared it to other capturing processes. His work suggested that greater efficiency can be obtained by avoiding more conservative assumptions. (Martin et al., 2011) evaluated the performance of hyper cross-linked polymers for CO_2 adsorption. This work concluded that the polymers were superior of zeolite-based materials and activated carbon in the CO_2 uptake. Furthermore, these polymers showed acceptable selectivity of CO_2 and low heat adsorption.

(Schell et al., 2012) tested the adsorption of CO_2 using three different metal organic materials. Promising results were obtained when comparing *USO-2-Ni* metal organic framework to activated carbon. Moreover, adsorption was also studied by (García et al., 2011) where partial pressure of CO_2 was the major factor in the capturing process using activated carbon. On the other hand, (Casas, Schell, Joss, & Mazzotti, 2013) studied pressure swing adsorption and

evaluated multiple process configurations and conditions to obtain better separation. It was concluded that decreasing the temperature and adsorption pressure would increase the separation efficiency.

Another study investigated air blown gasification rather than oxygen blown gasification and the plant efficiency was competitive (Moioli et al., 2014). The evaluation of mesoporous amine titanium oxide as a sorbent was done by (Jiang et al., 2015) and showed good stability and regeneration without loses, however, it is very expensive material. Absorption processes also took place in pre-combustion carbon capturing as (Ho, Jong, Wook, Nam, & Bin, 2014) designed two stage pre-combustion CO_2 units using physical absorbents. From an energy consumption point of view, Selexol was the most efficient in CO_2 capturing. Iconic liquid-based membrane was investigated at high pressure and temperature and it was noticed that the membrane contactor efficiency was decreasing with the increasing of its wetness (Dai & Deng, 2016).

Three studies investigated the hydrate-based gases for separation of CO_2 in pre-combustion capturing. (Babu, Wen, Ong, & Linga, 2016) concluded that tetrahydrofuran is better than other semi-clathrate hydrate formers. On the other hand, tested a combination of 5% *TBF* and 10% *TBAB* and discussed why it is the suitable choice of hydrate- based gas separation process (Yang, Jing, Zhao, Ling, & Song, 2016). Furthermore, (Zheng, Zhang, & Linga, 2016) illustrated the use of CO_2-H_2-*TBAF* as a promoter to increase CO_2 gas uptake at ambient temperature.

2.3 Oxyfuel Combustion Capture

In oxyfuel combustion, fuel is burnt in a nitrogen free environment. This is different than the conventional combustion which occurs in regular air. The products of oxyfuel combustion are mainly water and CO_2 where it does not require higher state of separation. The nitrogen in the air acts as a temperature moderator and its absence in oxyfuel combustion results in high flames' temperature. This is overcome by recycling part of the carbon dioxide to the combustor

with pure oxygen to keep the temperature within acceptable limits. Steam can also be injected in the combustion chamber as an alternative to reduce the mediums temperature. The water is collected from the products of the combustion by condensation and carbon dioxide is purified and compressed and prepared for transportation and storage (Sifat & Haseli, 2019).

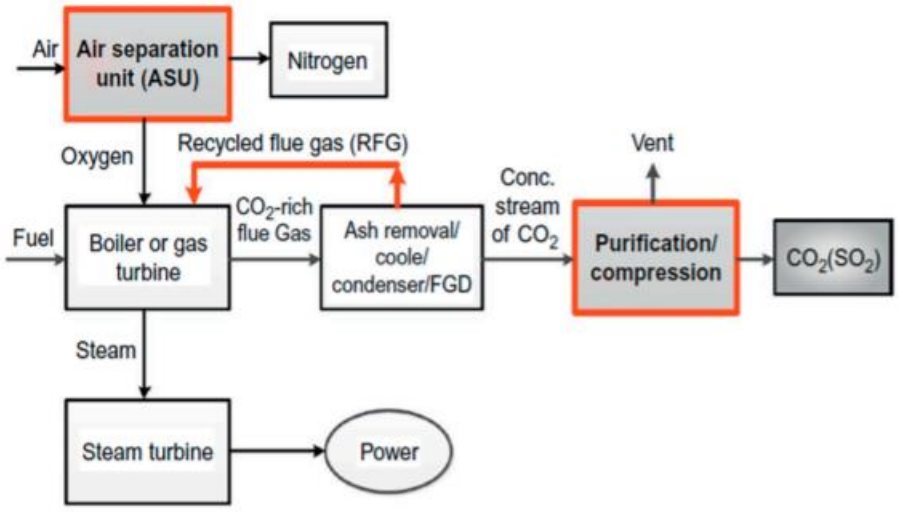

Figure 6: Oxyfuel combustion capturing process sequence. (Sifat & Haseli, 2019)

The oxyfuel combustion is considered a great method for carbon dioxide capturing for several reasons. For instance, burning fuels in a nitrogen free environment saves significant amount of heat that is absorbed by nitrogen in conventional combustion. Furthermore, in oxyfuel there is no or much less nitrogen oxides (NO_x) produced and no other pollutants in the combustion products. However, the cost of producing pure oxygen and compressing carbon dioxide is high, this is the main disadvantage of oxyfuel. A lot of research has been done on oxyfuel combustion and scientists argued that using membranes for separation is more economical than cryogenic methods. Adsorption technologies are yet to be implemented on large scale separation (Sifat & Haseli, 2019).

The integration of oxyfuel combustion with carbonation using $Mg(OH)_2$ to capture carbon dioxide was discussed by (Said, Eloneva, Fogelholm, & Fagerlund, 2011). The effect of Sulphur on oxyfuel combustion was investigated and reported its impact on furnace, ash

collection, carbon dioxide compression and transportation and storage (Stanger & Wall, 2011). (Chen, Yong, & Ghoniem, 2012) compared the oxyfuel combustion process to post combustion capture and reported a 1-5% less loss of efficiency in oxyfuel. This study also concluded that higher partial pressure in oxyfuel combustion resulted in higher absorption and emissivity of the flue gas. Furthermore, the ignition delay in oxyfuel is longer than other conventional combustion systems.

Other researchers studied the effect of recycling carbon dioxide to the combustion chamber. (Chen et al., 2012) mentioned the decrease in burning velocity and flame temperature when cycling carbon dioxide to the combustion chamber instead of the presence of nitrogen. (Oh & Noh, 2012) found that the flame speed of methane in oxyfuel is faster than air fuel combustion environment which contradicts Chen's study. (Mazas, Lacoste, & Schuller, 2016) tested the injection of water vapour effect on the speed of flame propagation and observed an increase in the molar fraction of steam decreased the flame velocity even at high rate of dilution. Moreover, the reduction of burning velocity for air combustion was larger than oxyfuel combustion as the steam molar fraction increase. (Xie et al., 2013) conducted experimental and numerical study on increasing carbon dioxide fraction in oxyfuel combustion and reported the reduction of flame speed, however, methane radiations were much higher.

The effect of ignition, stability of flame and flame extinction in oxyfuel combustion was studied by limited number of researchers. A detailed experiment by (Koroglu, Pryor, Lopez, Nash, & Vasu, 2016) testing methane in an oxyfuel environment was conducted. It was found that ignition delay is longer when methane is burnt in oxygen/carbon dioxide environment than oxygen/nitrogen environment. The pressure was varied from 1 to 4 atm and a temperature range of 1577 K to 2144 K in a shock tube facility. Similar experiment by (Pryor et al., 2017), sensitivity analysis showed that CO_2 could slow the overall rate of reaction and increase the ignition delay. This experiment was carried at pressure range of 6-31 atm and temperature of 1300-2000K.

(Allam et al., 2013) proposed a novel approach for power generation combined with oxyfuel combustion. This approach is basically a Brayton cycle with pressurized supercritical CO_2 as the working fluid. The study discussed the effect of high-pressure carbon dioxide on heat capacity and reported that condensing or vaporizing of water through the cycle is not important. The cycle begins with burning fuel in pure oxygen environment at a high-pressure combustor to produce a feed stream with pressure of ~ 300 bar. The feed stream passes through a turbine and expanded with a pressure ratio of 6 to 12 and the heat of the turbine's exhaust is transferred to recycled CO_2 stream in a recuperator. As discussed before, the recycled CO_2 stream controls the temperature of the combustion chamber. A 59% (*LHV-based*) thermal efficiency was reported for using natural gas as a fuel, and 52% efficiency using coal as a fuel. The schematic of Allam cycle is shown below (Allam et al., 2013).

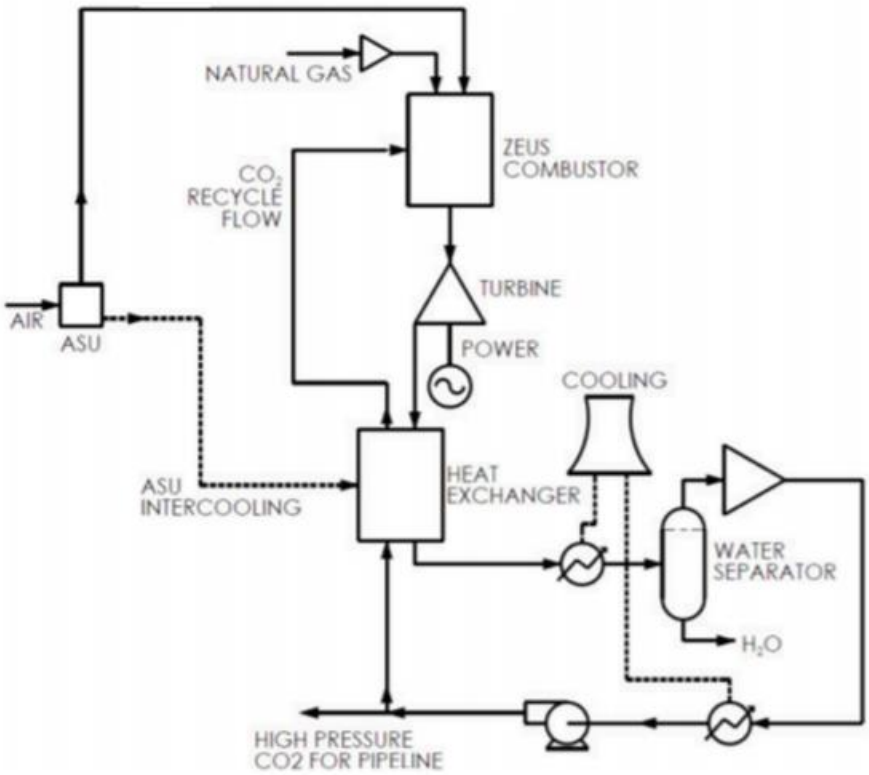

Figure 7: Allam cycle illustration. (Allam et al., 2013)

2.4 Post Combustion Capture

For post combustion, the capturing unit is installed in an existing power plant without significant changes of the plant. This is the main advantage of post combustion carbon capture when compared to oxyfuel and pre-combustion techniques. CO_2 is removed from the flue gases of the power plants which exists normally at atmospheric pressure. The concentration of carbon dioxide is usually in the range of 8-20 % which makes it very low. This variation in the carbon dioxide concentration is due to burning different types of fuels, for instance, burning coal produces flue gas that contains approximately 14% CO_2. However, burning natural gas can produce up to 40% if partial oxidation is used. This low percentage makes capturing CO_2 a challenge since the driving force is low and the cost of energy required is high (Sifat & Haseli, 2019).

Furthermore, the presence of impurities such as fly ash, SO_x and NO_x causes the separation process to be costlier with the current available technologies. Another challenge is designing the equipment for post combustion capture must be specific for each power plant as they differ in sizes and capacity (Sifat & Haseli, 2019). The unit must be designed to withstand high pressure and temperature environment. Many research studies suggested methods of cleaning the flue gas before capturing carbon dioxide. For example, (Merkel, Lin, Wei, & Baker, 2010) proposed passing the flue gas first to an electrostatic precipitator (*ESP*) to remove all large particles. A flue gas desulfurization unit (*FGD*) unit is required next to remove the sulphur content from the flue gas. Finally, a post combustion capturing unit is added to remove CO_2 and the remaining component of the flue gas at this stage would be mainly nitrogen.

In a combined cycle post combustion capturing unit with a natural gas power plant, a gas turbine expands the product of combusting natural gas with compressed air to produce electrical power. The high temperature from the turbine's exhaust is used to produce steam and this steam is used to generate additional power. Then flue gas is cooled and send to the CO_2 capturing unit. Amine based absorbent such as *MEA* and *MDEA* scrubs carbon dioxide from the flue gas in the absorber column leaving the treated gas to the exhaust (Sifat & Haseli, 2019).

The rich solvent is later stripped, and the solvent is regenerated in the desorber column where it is recycled back to absorber column and pure CO_2 is collected as the top product of the stripper. Carbon dioxide is compressed for storage and transportation to be used in other applications.

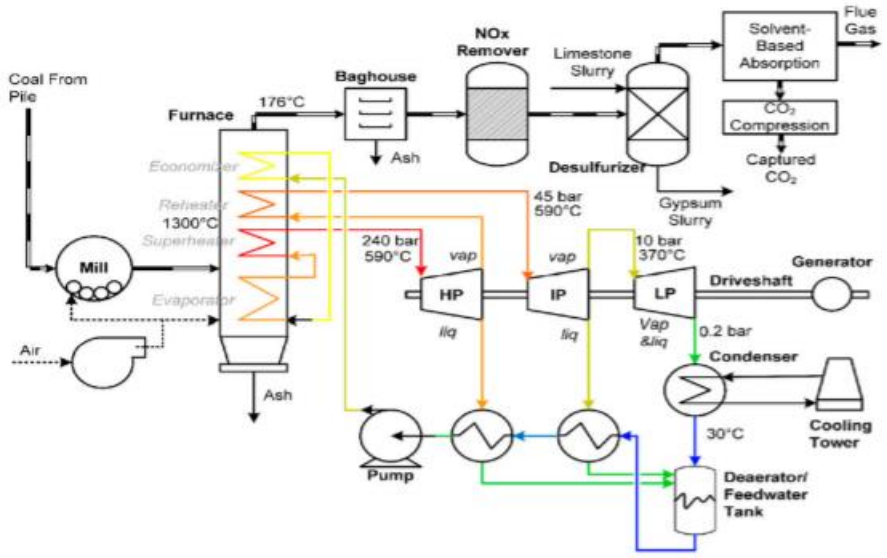

Figure 8: Coal-fired power plant with a post combustion unit. (Sifat & Haseli, 2019)

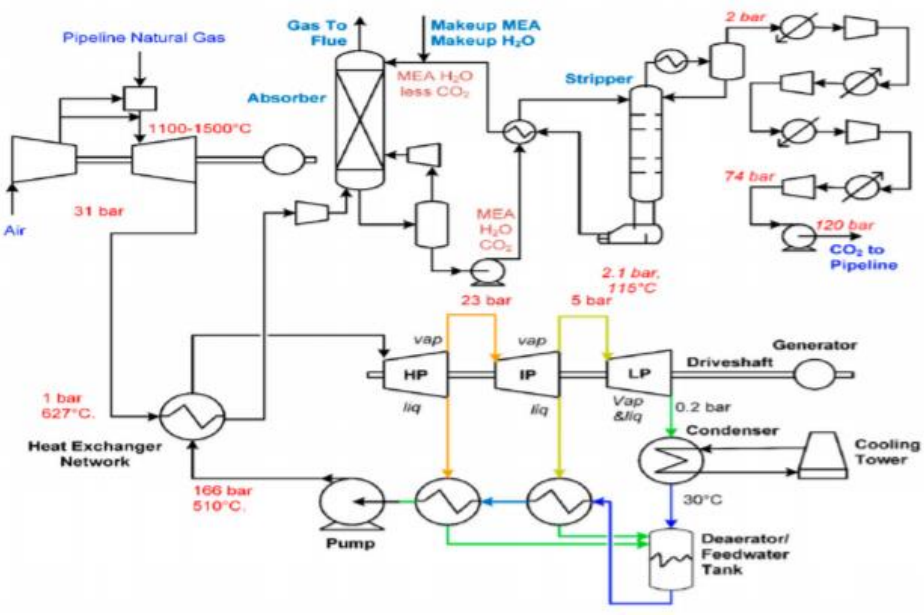

Figure 9: Natural gas power plant with a post combustion unit. (Sifat & Haseli, 2019)

(Merkel et al., 2010) discussed the use of high permeable membranes as a separation method and used incoming combustion air as sweep gas in a novel process. This study also emphasized the high permeance of the membranes rather than selectivity. In another study, pressure swing adsorption superstructure was presented to evaluate the optimality of carbon dioxide capturing cycle. The novel superstructure predicted the pressure swing adsorption performance up to 98%. (Wappel, Gronald, Kalb, & Draxler, 2010) compared the performance of pure and diluted iconic liquids to *MEA* in the absorber column and one of the iconic liquids showed lower energy requirement for the overall capturing process.

(Environ, Mason, Sumida, Herm, & Long, 2011) tested two *MOFs* as adsorbents for the post combustion process integrated with *PSA*. The presence of a strong carbon dioxide adsorption site such as Mg_2 (*dobdc*) is essential for *MOFs* to result in higher capturing rate. Biotechnology as a separation method took place in post combustion capture process where (Savile & Lalonde, 2011) used carbonic anhydrase derived from thermophiles to catalyze the process. Furthermore, nanomaterials as adsorbents showed high performance in capturing CO_2 due to the high surface area and the ability to adjust their properties, however, the cost of preparing and producing such materials is high (Z. H. Lee, Lee, Bhatia, & Mohamed, 2012).

(Scholes, Ho, Wiley, Stevens, & Kentish, 2013) suggested the modification of multiple membrane stages and cryogenic separation to increase the capturing efficiency. The cost was comparable to the current available technologies. (Bae et al., 2013) evaluated several zeolites as adsorbents such as *Ca-A*($Na_{0.28}Ca_{0.36}AlSiO_4$) which gave the highest uptake for carbon dioxide. The authors in (Brettschneider, Thiele, Faber, Thielert, & Wozny, 2004) developed a heat and mass transfer model to illustrate the absorption of carbon dioxide in a solution of sodium hydroxide, *MEA* and *MDEA*. The model was validated using experimental data. (Liu, Yu, Yuan, Liu, & Guo, 2006) proposed a complex computational mass transfer model of an

absorption packed column and considered the heat effect for prediction of the temperature and concentration profiles.

Computational fluid dynamics (*CFD*) was coupled with computational heat transfer (*CHT*) model validated with experimental data from a pilot packed tower to capture CO_2 from air using *MEA* as a solvent. Furthermore, (Lawal, Wang, Stephenson, & Yeung, 2009)developed a dynamic model of a post combustion CO_2 capture with *MEA* and compared two different approaches, equilibrium-based versus rate-based. The study concluded that the rate-based model gave better prediction of the absorption process. On the other hand, (Nittaya, Douglas, Croiset, & Ricardez-sandoval, 2014) proposed a dynamic model of an industrial scale CO_2 capture plant using *MEA* as a solvent. Three control structures were proposed to maintain a capturing rate above 87% when disturbances to the system are introduced.

(Behbahani, Jazayeri-rad, & Hajmirzaee, 2009) used neural networks to detect and diagnose faults in a sour gas absorption column. Variations in feed conditions were made to observe the changes in CO_2 captured, temperature and pressure drop. The performance of back propagation neural networks and radial basis function (*RBF*) to simulate pilot scale packed absorption column was compared in (Shahsavand, Fard, & Sotoudeh, 2011). The study showed that *RBF* networks performed more efficiently. The authors in (Li, Sharma, Khalilpour, & Abbas, 2013) developed a methodology to determine the optimal operating conditions of a solvent-based post combustion carbon capture with a techno-economical objective. Around 1700 case studies were used to develop a reduced model of the *PCC* unit and the optimal values were used as control set points for the plant.

Another study by (Chan & Chan, 2017) illustrated the application of piece-wise linear artificial neural networks (*PWL-ANN*) on a carbon dioxide capture process system dataset. The study indicated the key process parameters to be steam flow rate through reboiler, reboiler pressure and the CO_2 concentration in the flue gas. The performance of artificial neural networks (*ANN*), least-square support vector machine (*LSSVM*), and adaptive neuro-fuzzy inference system

(*ANFIS*) models with AdaBoost-CART algorithm was compared by (Ghiasi, Abedi-farizhendi, & Mohammadi, 2019). These models predicted the equilibrium data of a carbon dioxide absorption column using monoethanolamine (*MEA*), diethanolamine (*DEA*) and triethanolamine (*TEA*).

2.5 Machine Learning

Machine learning and artificial intelligence are widely used terms nowadays and have proven to be powerful tools in the field of technology and data analysis. Several successful applications of machine learning such as handwriting and speech recognition, image classification, demand forecasting and spam filtration, are used daily by billions of users (J. H. Lee, Shin, & Realff, 2018).

Machine learning is classified into four classes, supervised, unsupervised learning, semi-supervised learning, reinforcement learning. In the first class, the software learns to predict the relationship between labelled inputs and outputs data which is used in classification and regression applications. While in unsupervised learning, unlabelled data are used to determine the distribution which is used in feature extraction and clustering. On the other hand, semi-supervised learning gained much attention in the past few years as it uses unlabelled data in the probability distribution learning process and then optimizes the predictions over labelled and unlabelled data in a combined objective. Finally, the reinforcement learning uses critic and inputs data to learn the optima relation between inputs and outputs or the relation between inputs and performance index. Reinforcement learning is considered to be the best choice for many applications as it combines online learning and self-optimization characteristics (J. H. Lee et al., 2018).

When it comes to process system engineering (*PSE*), machine learning plays a great role in solving many problems such as nonlinear principle component analysis (*PCA*), learning time series hierarchal features for monitoring and diagnosis, planning and scheduling, control and uncertain mapping and dynamics (J. H. Lee et al., 2018). One of the earliest applications of machine learning is the invention of auto-encoder (*AE*), which is an artificial neural network that represent encoding of a data set, as in *PCA* dimensionality reduction of data is achieved. (Kramer, 1991) introduced auto-associative neural networks (*AANN*) which compresses and encodes the inputs data in the middle layer of the network and refer to this application to be a nonlinear *PCA*. This neural network was trained to predict the mapping between inputs and outputs. the major drawback of this approach was the difficulty of training the network using back propagation algorithm which caused the error gradient to become zero in the first few layers. (Chatterjee, 2000) also introduced technique in nonlinear model reduction based on *PCA* called proper orthogonal decomposition (*POD*). This technique was used to reduce the dimensionality of discretized fluid flow equations.

The integration of planning and scheduling is a long-standing problem in *PSE* since high- level decision problems (planning) has recurring dynamics and uncertainties are dominating the problem and a stochastic dynamic programing is required to solve the problem. Furthermore, scheduling which is considered to be a low-level decision problem has more complex state representation, and mathematical programing is suitable to solve these kinds of problems. Combined planning and scheduling problems are studied, and potential approaches has been discussed by (J. H. Lee & Min, 2006; Shin, Lee, & Realff, 2017).

Chapter 3: Modelling

3.1 System Description

The post-combustion carbon dioxide capturing unit includes two main components: an absorber and a stripper column. The flue gas which is loaded with carbon dioxide is feed to the absorber column from the bottom and the solvent is feed from the top of the column. In this work mono-ethanolamine (*MEA*) is used as a solvent to absorb the CO_2 from the flue gas. The flow mechanism in the absorber is counter current and packed columns are used sometimes to increase the surface contact area between the gas and the liquid. The rich *MEA* solution is accumulated in the absorber sump tank before flowing to the heat exchanger. The rich solvent is feed to the stripper from the top and encounters the steam produced from the reboiler. CO_2 is separated from the *MEA* solution and comes from the top of the desorber after being cooled by a condenser. The regenerated amine solution (free from CO_2) is the bottom product passes through the heat exchanger. The lean amine is sent to a make-up tank where the water and *MEA* loses are recovered before flowing back the absorber column. The collected CO_2 then is ready for transporting and storage (Nittaya, 2014).

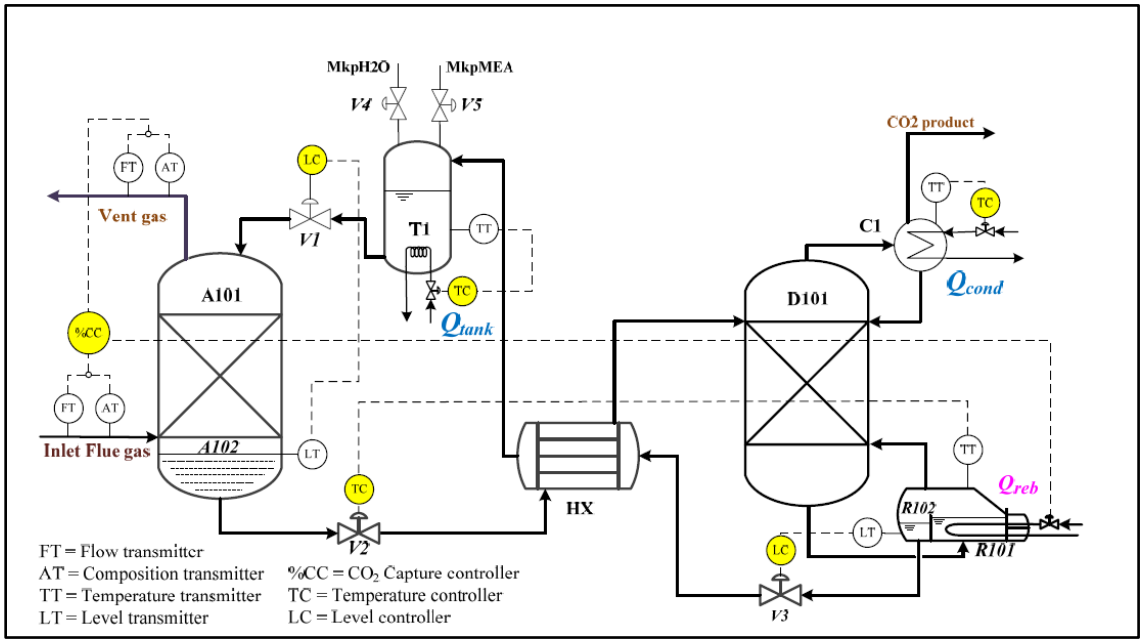

Figure 10: Post combustion unit schematic. (Nittaya, 2014)

The rigorous model used in this work was developed by (Nittaya, 2014) and (Harun, 2012). It was built and simulated in gProms v5.1 using six PI controllers; the manipulated and controlled variables are illustrated in the following table with the nominal steady state operating values.

Table 1: Manipulated and controlled variables of the post combustion system. (Nittaya, 2014)

Variable		**Nominal Value**
Manipulated variable (1)	Condenser heat duty (Q_{cond})	8.6 kW
Manipulated variable (2)	Buffer tank heat duty (Q_{tank})	164.3 kW
Manipulated variable (3)	Reboiler heat duty (Q_{reb})	153.6 kW
Manipulated variable (4)	Outlet buffer tank valve (*V1*)	32% opening
Manipulated variable (5)	Outlet absorber sump valve (*V2*)	50 % opening
Manipulated variable (6)	Outlet reboiler sump valve (*V3*)	50 % opening
Controlled variable (1)	Condenser temperature (T_{cond})	313.8 K
Controlled variable (2)	Lean amine temperature (T_{tank})	312.8 K
Controlled variable (3)	Reboiler temperature (T_{reb})	388.45 K
Controlled variable (4)	Percentage CO_2 removal (*%CC*)	96.3 %
Controlled variable (5)	Liquid level in absorber sump (*L2*)	0.3 m
Controlled variable (6)	Liquid level in reboiler sump (*L3*)	0.3 m

The design parameters of the units which includes dimensions, operating temperature and pressure for the model are illustrated below.

Table 2: Equipment design parameters. (Nittaya, 2014)

Parameter	**Value**	**Model**
Absorber (A101)		
Internal diameter (m)	0.43	(Nittaya, 2014)
Height (m)	6.1	(Nittaya, 2014)
Packing	IMTP#40	(Nittaya, 2014)
Nominal packing size (mm)	0.038	(Nittaya, 2014)

Specific area (m^2/m^3)	143.9	(Nittaya, 2014)
Operating temperature (K)	314-329	(Nittaya, 2014)
Operating pressure (kPa)	101.3 – 103.5	(Nittaya, 2014)
Stripper (D101)		
Internal diameter (m)	0.43	(Harun, 2012)
Height (m)	601	(Harun, 2012)
Packing	IMTP#40	(Harun, 2012)
Operating temperature (K)	350-380	(Harun, 2012)
Operating pressure (kPa)	159.5 – 160	(Harun, 2012)
Reboiler (R101)		
Operating temperature (K)	383-393	(Harun, 2012)
Operating pressure (kPa)	160	(Harun, 2012)
Condenser (C1)		
Operating temperature (K)	312-315	(Nittaya, 2014)
Operating pressure (kPa)	159	(Nittaya, 2014)
Cross heat exchanger (HX)		
Internal diameter of shell (m)	0.305	(Nittaya, 2014)
Internal diameter of tube (m)	0.148	(Nittaya, 2014)
Outer tube diameter of tube (m)	0.19	(Nittaya, 2014)
Buffer tank (T1)		
Internal diameter (m)	2	(Nittaya, 2014)
Absorber sump tank (A102)		
Internal diameter (m)	0.43	(Nittaya, 2014)
Reboiler sump tank (R102)		
Internal diameter (m)	0.43	(Nittaya, 2014)
Valves		
Flow coefficient of V1 (m2)	1.01 * 10E-3	(Nittaya, 2014)
Flow coefficient of V2 (m2)	0.85 * 10E-3	(Nittaya, 2014)
Flow coefficient of V3 (m2)	0.85 * 10E-3	(Nittaya, 2014)

3.2 Sensitivity Analysis

The determination of system inputs and outputs for modelling purposes is essential. The system is analysed by studying the effect of changing input variables on the desired outputs. Many studies previously discussed the effect of changing different variables such as the flue gas flow rate, temperature, pressure, reboiler and condenser duty and lean amine flow rate and temperature. This analysis provides insights regarding the behaviour of the proves variables

and their effects on the process outputs. Furthermore, the design of the machine learning models will be depending on the selection of the important variables from the analysis. In this section, illustration of how inputs variables selected are affecting the system outputs. for steady state modelling, all controllers are turned off and the data is collected at the initial and final state.

First, the change of flue gas flow rate by ± 20% is investigated and shown in the figures below. Increasing the flue gas flow rate reduces the system energy requirements while it increases the purity of CO_2 produced by about 10%. This is justified as the post combustion unit treats more flue gas and higher amount of CO_2 is loaded to the system. Furthermore, as the flow rate of the flue gas increase, the capturing rate decreases but still within acceptable limit which is not below 90%. This is expected since the amount of the lean amine treating the flue gas is not changing as it is kept constant during the disturbances introduced to the flue gas flow rate.

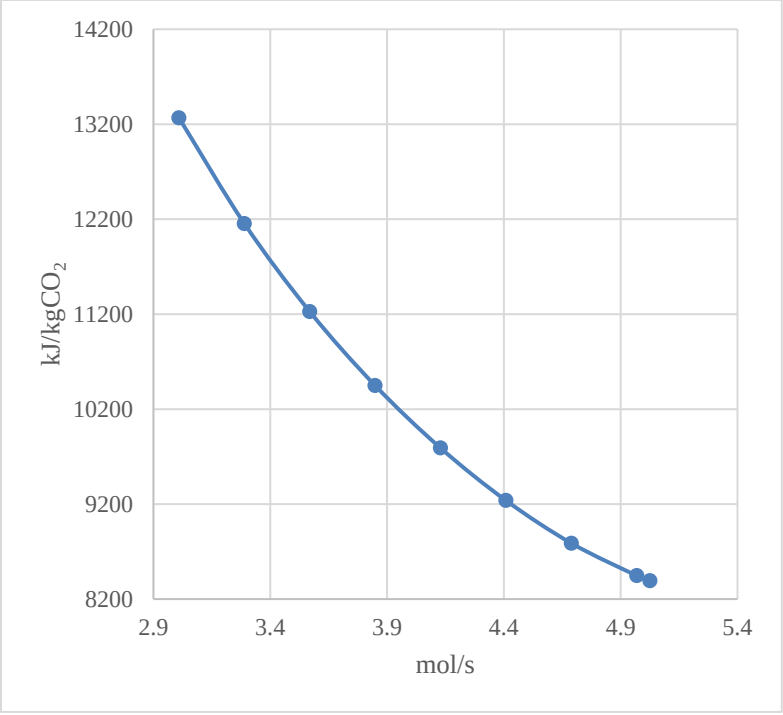

Figure 11: The effect of flue gas flow rate on *SER*.

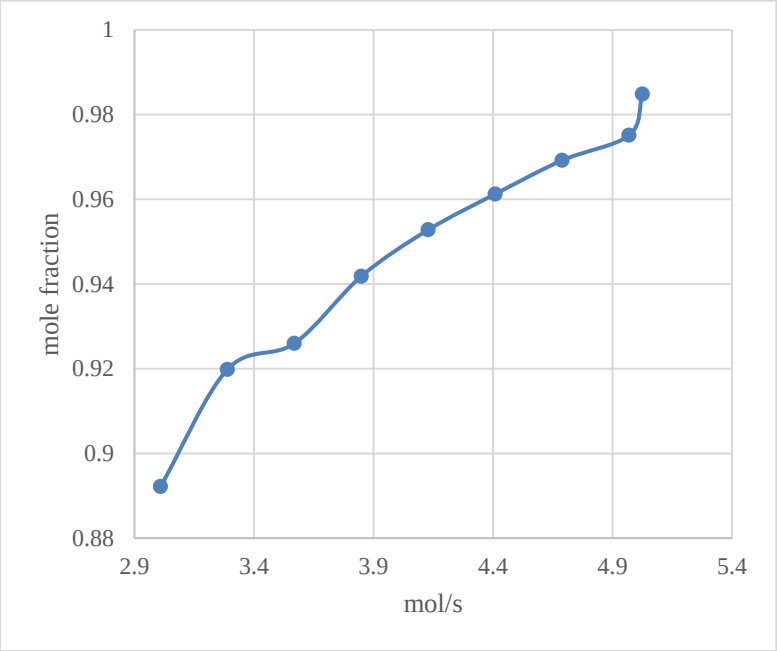

Figure 12: The effect of flue gas flow rate on purity.

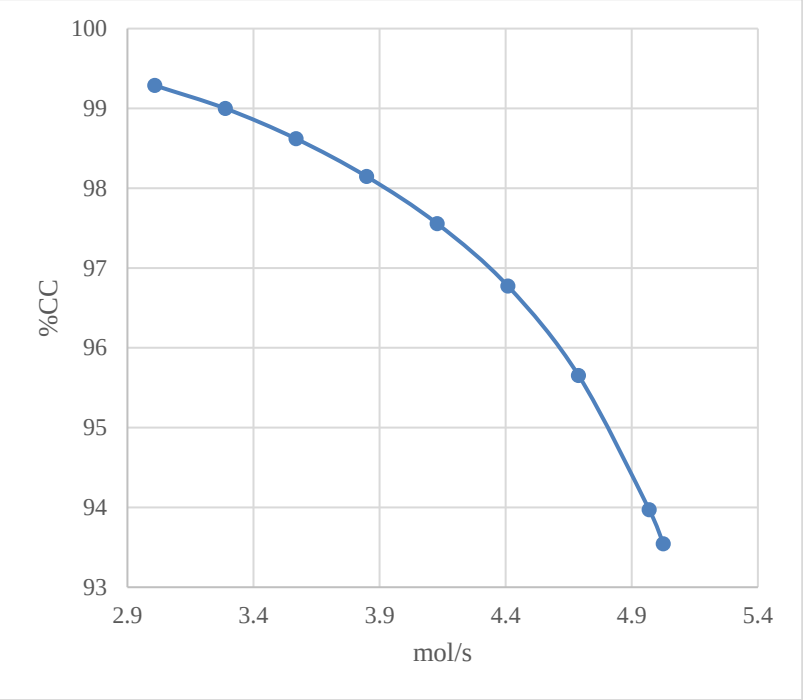

Figure 13: The effect of flue gas flow rate on capturing rate.

Secondly, the flue gas pressure was changed to 90 kPa which is 13% below the nominal value and increased gradually to reach 110 kPa which is about 6.5% above the nominal value. It was noticed that both *SER* and the purity of CO_2 decreased with the increase of the pressure. However, the change in the purity is very small. On the other hand, the capturing rate increased with the increase of the pressure. In real life, the change of the flue gas pressure would occur if blowers are used to feed the absorber. This will also affect the system energy requirement as the energy consumed by the blowers will be added. From the results it was noticed that the high-pressure flue gas requires low energy consumption by the system. This can be explained as the temperature of the flue gas will increase hence, less heating is required.

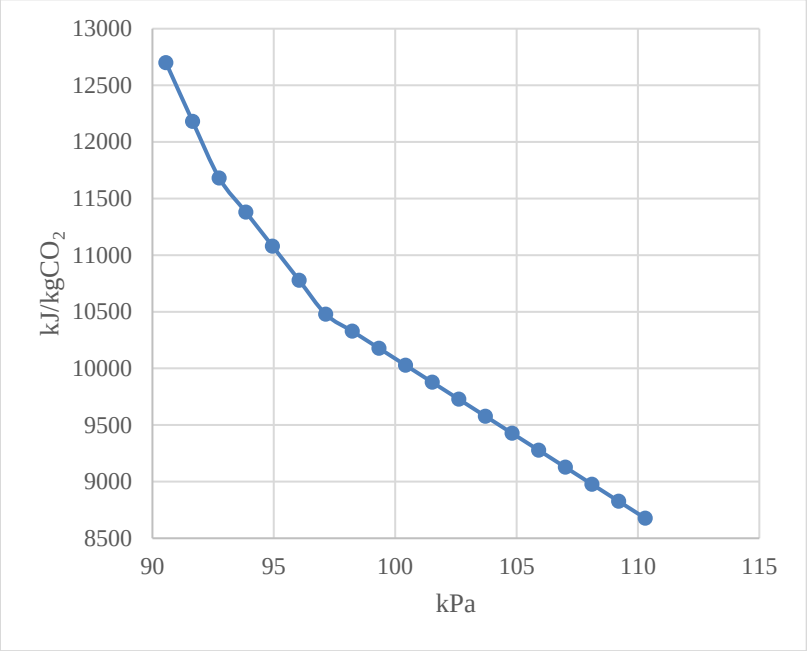

Figure 14: The effect of flue gas pressure on *SER*.

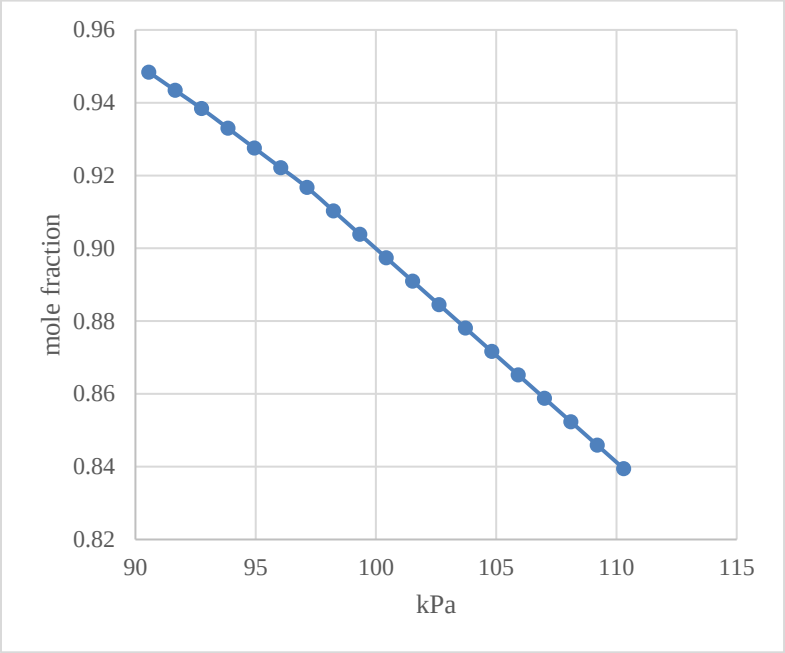

Figure 15: The effect of flue gas pressure on purity.

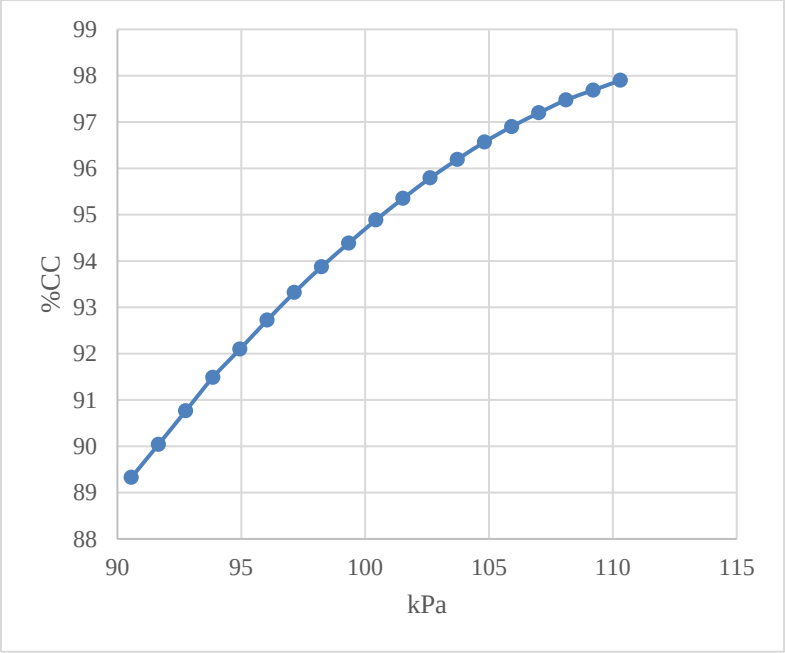

Figure 16: The effect of flue gas pressure on capturing rate.

The effect of changing the flue gas temperature was also investigated and a change of ± 20% was applied to the nominal value. As the temperature if the flue gas increases only the system energy requirement increases in a small matter which makes since as less heat is required through the process. While the purity and the capturing rate decreases with a change about 10%.

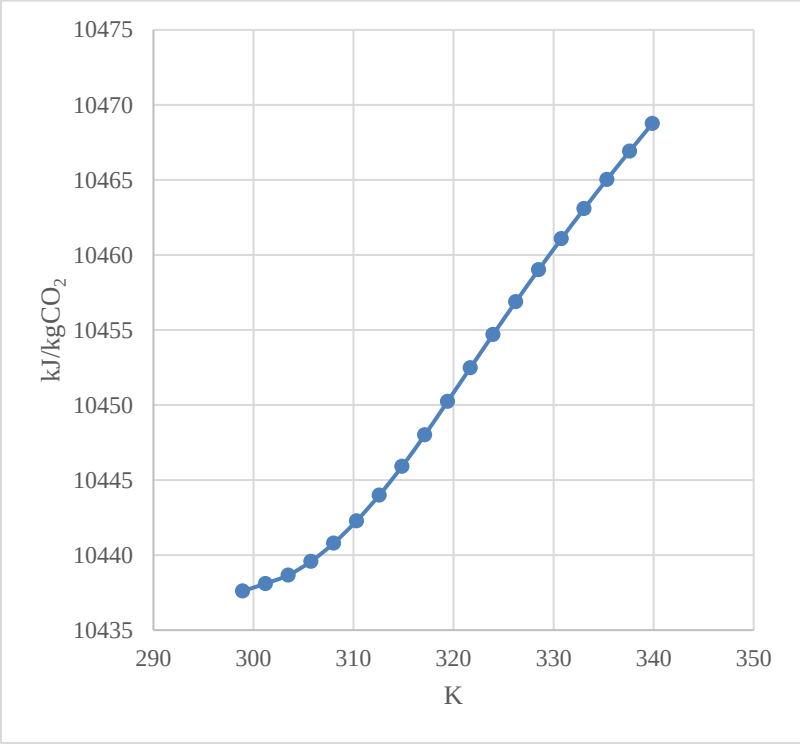

Figure 17: The effect of flue gas temperature on *SER*.

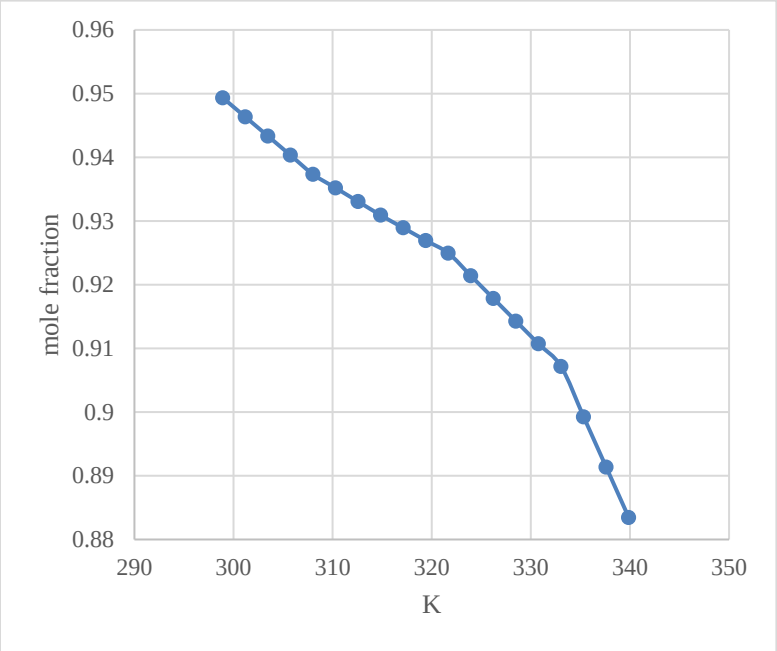

Figure 18: The effect of flue gas temperature on purity.

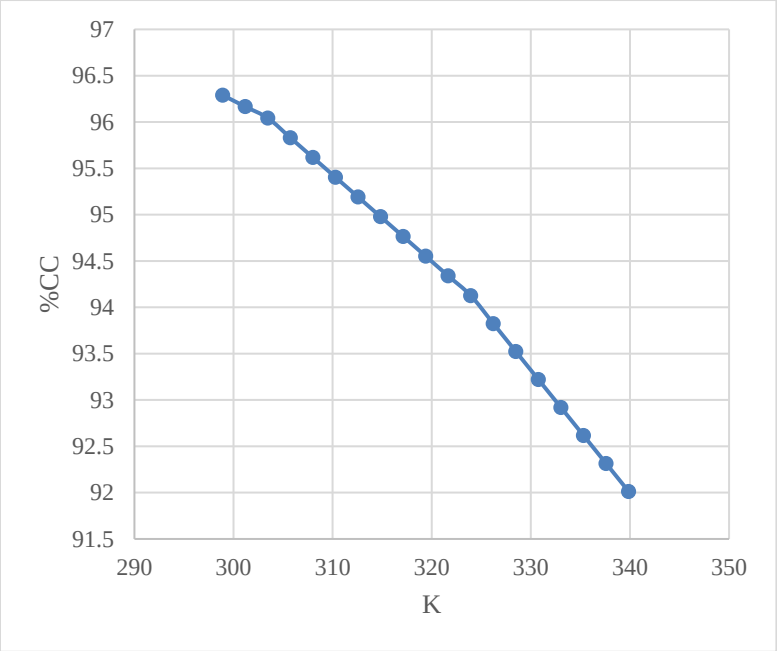

Figure 19: The effect of flue gas temperature on capturing rate.

Following the flue gas flow rate, pressure and temperature, the reboiler and condenser duty were also manipulated to observe their effect on the systems outputs. It is very clear that

increasing both the reboiler and condenser duty will increase the system energy requirement. However, when it comes to purity, it was noticed that increasing the reboiler duty would decrease the purity of CO_2 produced. On the other hand, increasing the condenser duty significantly increases the purity of CO_2 produced. Moreover, increasing the reboiler duty increased the capturing rate significantly. While increasing the condenser duty reduced the capturing rate but in a minor concern.

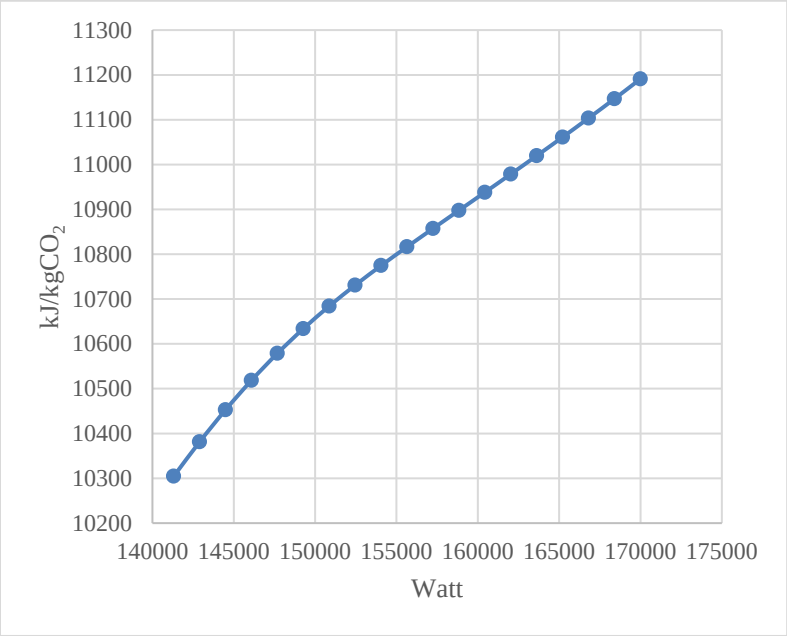

Figure 20: The effect of reboiler duty on *SER*.

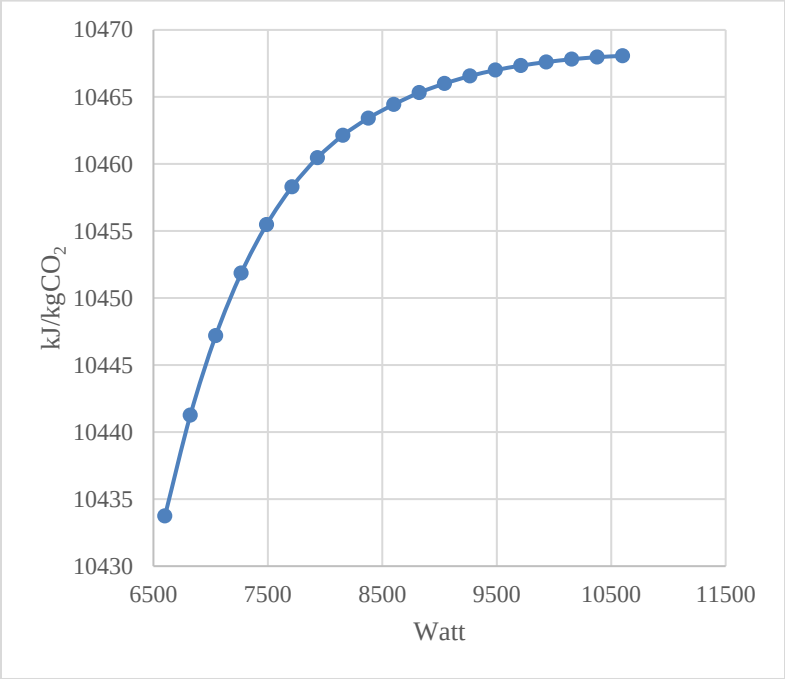

Figure 21: The effect of condenser duty on *SER*.

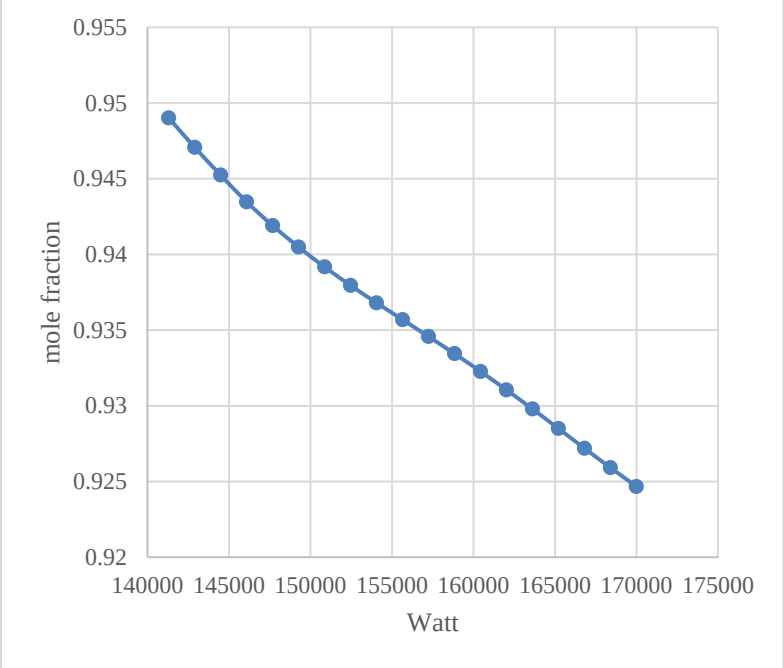

Figure 22: The effect of reboiler duty on purity.

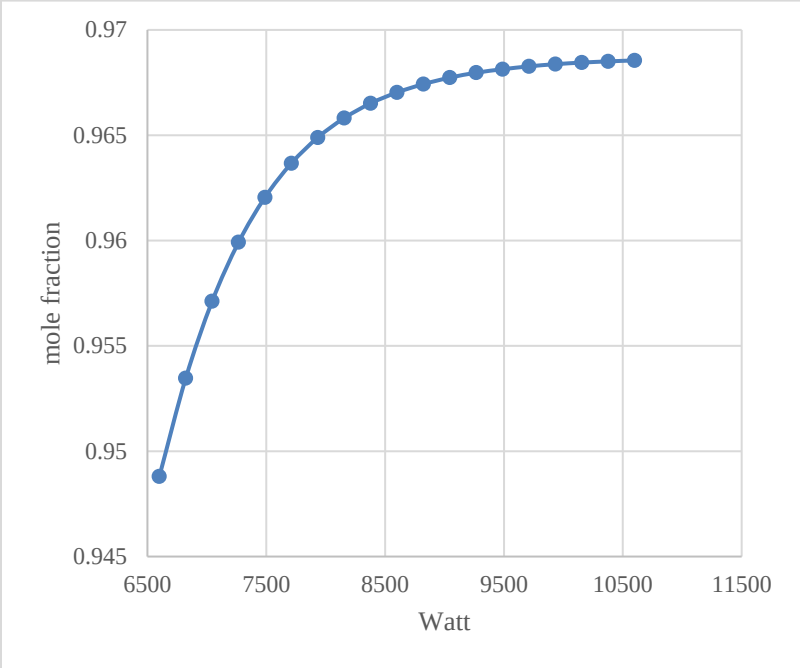

Figure 23: The effect of condenser duty on purity.

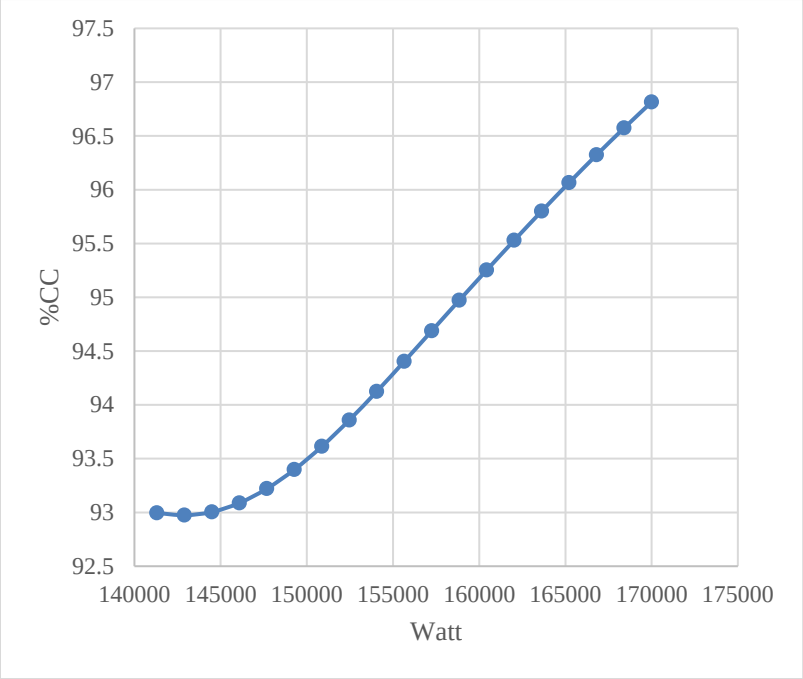

Figure 24: The effect of reboiler duty on capturing rate.

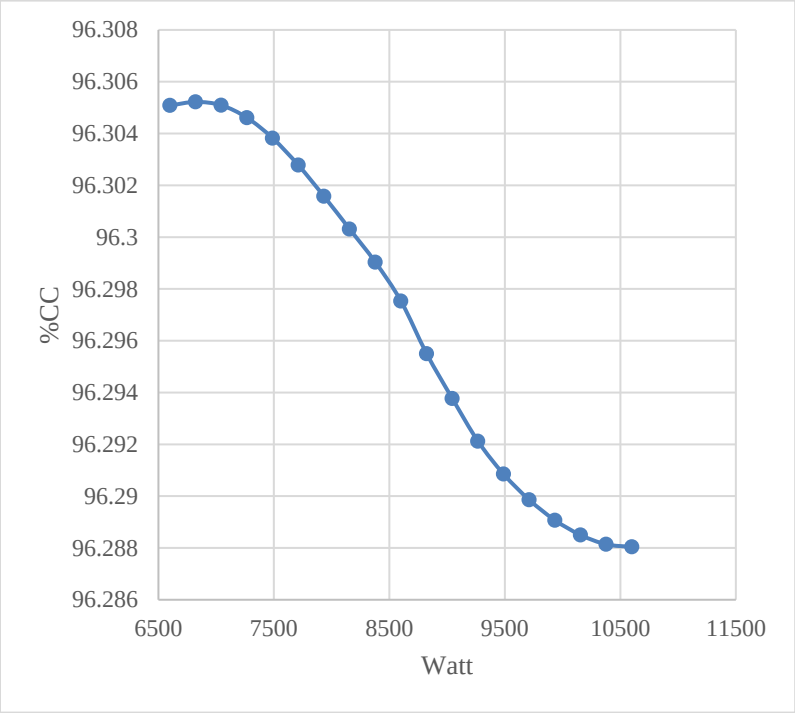

Figure 25: The effect of condenser duty on capturing rate.

3.3 Steady State Modelling

This section describes the development of different machine learning models for the *PCC* unit illustrated earlier. The inputs of the system represent the independent variables while the outputs are the dependent variables. In this section controllers are not involved as the initial and final state of each simulation is the point of interest. Six main inputs of the system were selected based on the literature and sensitivity analysis which are reboiler duty, condenser duty, reboiler pressure, flow rate, temperature and pressure of the flue gas. Table (3) illustrates the summary of the inputs and outputs chosen for the modelling with the upper and lower limits that this system can withstand.

Table 3: Inputs and outputs variables for steady state modelling.

Variable	Variable Name	Variable Type	Lower limit	Mid-Point	Upper limit
x_1	Flow Rate (mol/s)	Input	3.21	4.0125	5.13
x_2	Temperature (K)	Input	299	320	340
x_3	Pressure (kPa)	Input	95	103.5	110
x_4	Reboiler Pressure (kPa)	Input	140	160	180
x_5	Reboiler Duty (W)	Input	141312	158744	170000
x_6	Condenser Duty (W)	Input	6600	8600	10600
y_1	System Energy Requirements (kJ/kg CO_2)	Output	5239	12346	16345
y_2	Capture Rate %	Output	68.22	91.78	99.98
y_3	Purity	Output	0.55	0.867	0.9997

A change of ± 20% from the nominal value of each input was made to observe the outputs and system response. A combination of 324 scenarios were developed by taking into considerations an upper, mid and lower limit for each input. Three main outputs were chosen, which are the system energy requirement, the capture rate and the purity of carbon dioxide from the condenser outlet stream. The changes in the inputs of the system were done interchangeably, which means the disturbance was introduce to all the variables simultaneously to cover a wide range of the possible changes to operating conditions and to study the effect of these changes on the outputs of the process. The inputs and outputs and their limits are shown in table (3). *SER* describes how much energy is consumed by the reboiler (*R102*), make-up tank (*T1*) and the condenser (*C1*) in kJ per kg of CO_2 captured. The capture rate (*CR*) is defined as follows:

$$\%\, CR = \left(1 - \frac{y_{CO_2,out,Abs} \times F_{v,out,Abs}}{y_{CO_2,in,Abs} \times F_{v,in,Abs}}\right) \times 100\% \quad (4)$$

Where $y_{CO_2,out,Abs}$ and $y_{CO_2,in,Abs}$ are the mole fractions of CO_2 in the vent gas stream from the absorber and the flue gas stream going to the absorber, whereas $F_{v,in,Abs}$ and $F_{v,out,Abs}$ are the molar flow rates of the flue gas and the vent gas stream respectively.

3.3.1 Artificial Neural Network (ANN)

Artificial neural networks are also known as multilayer perceptron (*MLP*), they are defined by a single input layer with *R* inputs, *M* – 1 hidden layer and in each layer a number of neurons S^m and an output layer with S^M neurons which correspond to the number of outputs of the network. An example notation describing the *MLP* is nn = [R S^1 S^2 ... S^M]. For instance, a neural network with three inputs, three hidden layers and one output would be nn = [3 3 3 1].

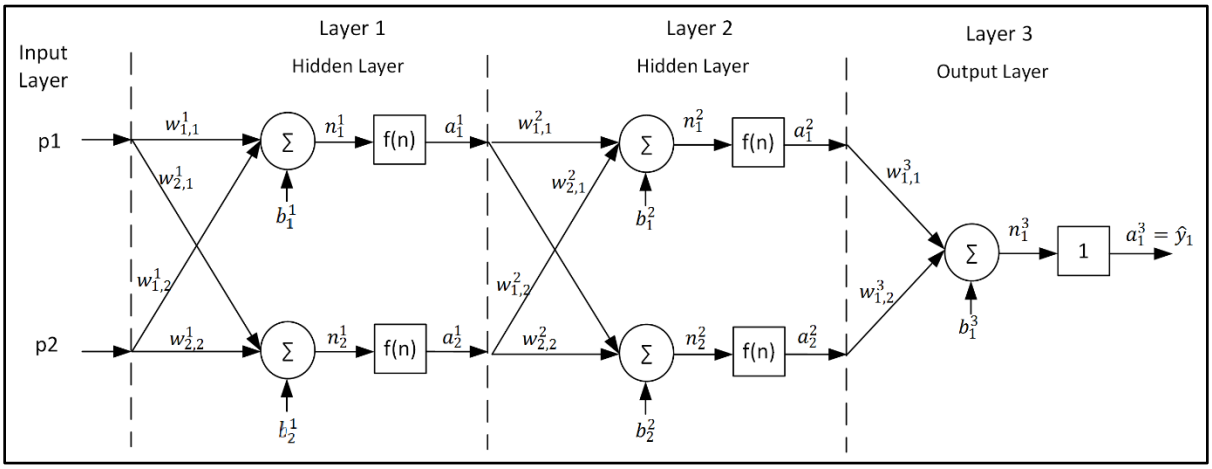

Figure 26: ANN configuration (Feed forward neural networks in pyrenn).

The *ANN* model can be described as a black box device that receives inputs and produces outputs (Elkamel, 2006). A wide range of neural network architectures is available to serve different types of applications. The *ANN* used in this work is a typical feed-forward model consisting of an input layer, hidden layers and an output layer. The structure of the *ANN* is shown in figure (27). Each layer consists of neurons, and connections between neurons in different layers are associated with a weight factor (Chan & Chan, 2017). The weight and bias for the *ANN* were determined using a back-propagation algorithm with momentum. The data were divided into two sets, the training set (70%) and the testing set (30%). The training step assures that the weights leads to the least sum of squared errors (*SSE*) between the actual

outputs and the predicted ones. The training is performed to achieve an *SSE* of 10^{-5}. Moreover, the data are normalized before training, so the inputs and outputs have the same order of magnitude.

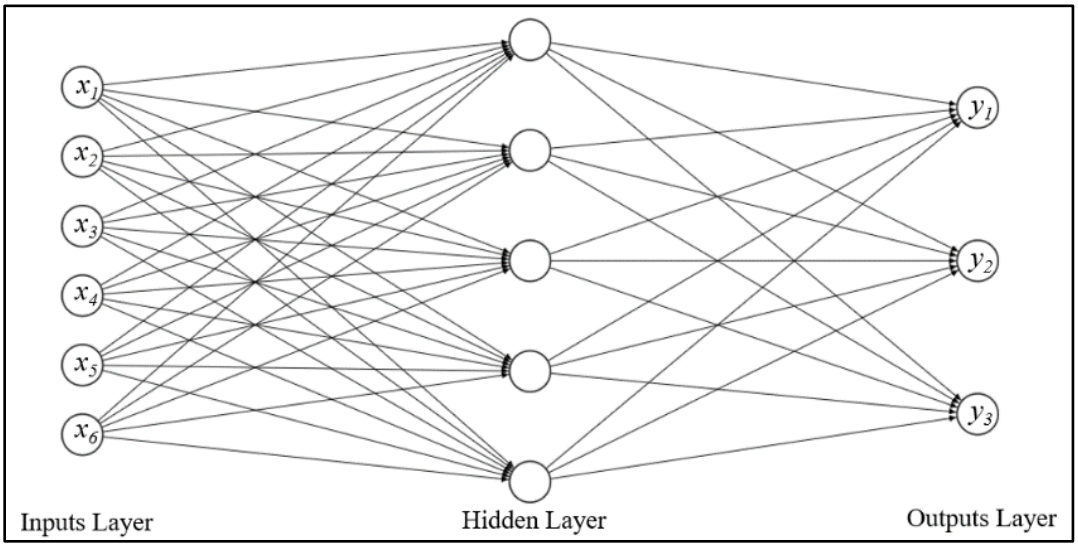

Figure 27: ANN structure with single hidden layer.

A sigmoid function was used as an activation function for the hidden layer neurons. The hidden layer network with 5 neurons was able to give good predictions of the process outputs. The minimum, maximum and average errors calculated along with the coefficient regression for statistical analysis were calculated. It is noticed that the performance of the trained network is pleasant.

3.3.2 Gaussian Process Regression (GPR)

In comparison to *ANN*, Gaussian process regression is also used to model the post combustion system. The *GPR* model is also used to predict the system outputs using the same inputs of the *ANN*. Gaussian process regression (*GPR*) is one of the most reliable machine learning models. It is a supervised learning method designed to solve probabilistic regression and probabilistic classification problems (Seeger, 2004). *GPR* is a powerful tool capable of predicting the outputs of a system based on the interpolation of the observations. Furthermore, the predictions

are probabilistic which means that empirical confidence intervals can be computed to decide refitting the model or adjusting it. Different kernels can be used, however, *GPR* models are not sparse and use the whole sample information for predictions. Another disadvantage of *GPR* is the low efficiency in high dimensional spaces. However, in this work, the system on hand is represented by 9 variables and *GPR* managed to fit the model with high efficiency and low error. *GPR* is specified by its mean and covariance functions, where the prior mean is assumed to be constant 0 or the data's mean. The prior's covariance is determined by passing a kernel object. Maximizing the log-marginal-likelihood (*LML*) optimizes the hyper parameter of the kernel. The simplest form of *GPR* model can be explained as follow:

$$y = x^T\beta + \varepsilon \tag{5}$$

Where $\varepsilon \sim N(0, \sigma^2)$ and y is the predicted response to a vector x. The error variance (σ) and the coefficient β are estimated from the data. The predicted response is explained by introducing latent variables, $f(x_i)$, i = 1, 2, …, n, from a Gaussian process, and a basis h. The covariance function of the latent variables detects the smoothness of the outputs and basis function projects the inputs into a p-dimensional feature space. In this work three different kernel functions were used in modelling the *PCC* unit. The first kernel used to predict the capturing rate (*CR*) and the purity of CO_2 (*PU*) is the rational quadratic *GPR* where the covariance function is defined by:

$$k(x_i, x_j, \theta) = \sigma_f^2 \left(1 + \frac{r^2}{2\alpha\sigma_l^2}\right)^{-\alpha} \tag{6}$$

Where σ_l is the characteristic length scale, α is a positive value scaled mixture parameter and r is the Euclidean distance between x_i and x_j. The second kernel used to predict the purity (*PU*) and capturing rate (*CR*) is the squared exponential *GPR* where the covariance function is:

$$k(x_i, x_j, \theta) = \sigma_f^2 \left[-\frac{1}{2}\frac{(x_i - x_j)^T(x_i - x_j)}{\sigma_l^2}\right] \tag{7}$$

Where σ_l is the characteristic length scale, and σ_l is the signal standard deviation.

Finally, a Matern 5/2 kernel was used to predict (*CR*) and (*SER*) and the covariance function is defined as:

$$k(x_i, x_j, \theta) = \sigma_f^2 \left(1 + \frac{\sqrt{5}r}{\sigma_l} + \frac{5r^2}{3\sigma_l^2}\right) \exp\left(-\frac{\sqrt{5}r}{\sigma_l}\right) \quad (8)$$

3.3.3 Tree Regression (Fine Tree)

Tree regression is another machine learning predicting tool that uses recursive partitioning for non-linear systems. It divides the space between leaves/nodes into smaller regions to make the interaction manageable. Each terminal node or leaf of the tree represents a cell of the partition. It can be viewed as a set of if-else statement to decide the output. Three types of trees exist depending on the size of the leaves, fine tree, medium tree and coarse tree. A fine tree model with 65 nodes was able to predict (*SER*) efficiently.

A statistical analysis in table (4) was conducted to compare the developed models and to demonstrate the most efficient ones. It is clear that the *ANN* models excelled all other developed models, hence, it is the most recommended model to be used for predictions as the accuracy was never below 98%. However, the other models showed high accuracy in predicting the process outputs. Moreover, the ANN model was able to predict all process outputs while all other models resulted in good predictions for at most two of the process outputs.

Table 4: Statistical analysis comparing accuracy of different steady state models.

Model	Output	Minimum Error	Maximum Error	Average Error	R^2
ANN	*SER*	0.00067	12.3186	0.18866	0.98108
Fine Tree		0.00017	15.1444	2.19788	0.96309
Matern 5/2 GPR		0.02025	15.5239	3.02674	0.95293
ANN	*CR*	0.00078	6.70323	0.87294	0.98414
Rational Quadratic GPR		0.01040	5.37134	1.07592	0.98269
Matern 5/2 GPR		0.00912	5.55021	1.12226	0.98152
ANN	*PU*	0.00155	8.04515	1.31160	0.98732
Squared Exponential GPR		0.00681	9.86385	1.68887	0.98186

Rational Quadratic GPR		0.00665	9.86387	1.68892	0.98186

3.4 Dynamic Modelling

This section illustrates the process of dynamic modelling for the *PCC* and what are the essential variables to be considered, and how are the system inputs and outputs are related. The *PCC* designed and modelled by (Nittaya, 2014) had a set of control objectives summarized as follows:

1. The removal rate of CO_2 should be 90% or higher.
2. The purity of CO_2 in the gas product stream leaving the condenser following the stripping column should be above 95%.

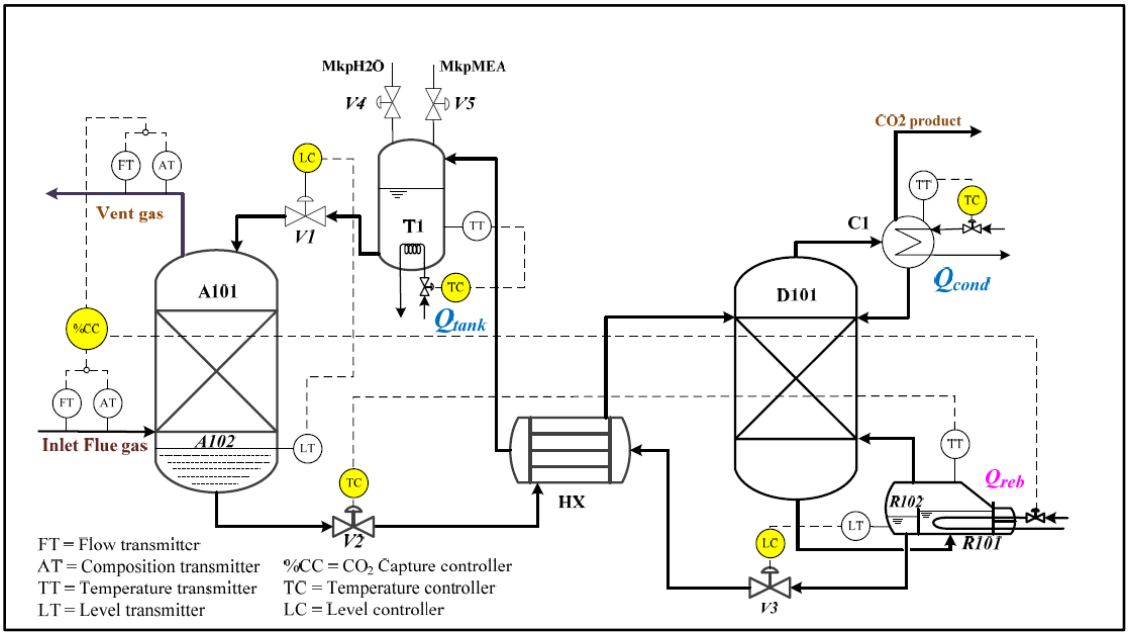

Figure 28: Post combustion unit control structure.(Nittaya, 2014)

The control structure of the *PCC* unit consists of six manipulated variables and six controlled variables. Three valves are manipulated and regulated to control cooling and heating mediums and the liquid level in the sump or surge tanks. For example, the valve ($V2$) is used to control the reboiler temperature (T_{reb}) by regulating the amount of liquid flowing through the reboiler.

On the other hand, valve (*V1*) control the liquid level in the absorber sump tank. This is beneficial due to the control of the amount of rich amine flowing to the absorber to guarantee sufficient CO_2 removal in case of the flue gas flow rate increased. Moreover, valve (*V3*) controls the liquid level in the reboiler tank (Nittaya, 2014). Furthermore, the reboiler duty (Q_{reb}) is used to control the %*CC*, while the condenser duty (Q_{cond}) controls the temperature of the condenser. Finally, the makeup tank temperature is controlled by adjusting the tank duty (Q_{tank}). The manipulation of the duties is essential to achieve the control objectives; however, it is challenging to maintain a low energy consumption to achieve the requirements. The previous schematic illustrates the control structure of the system, while table (5) is summarizing the controlled and manipulated variables with their set point.

Table 5: Manipulated and controlled variables of the post combustion unit. (Nittaya, 2014)

Manipulated Variables	**Steady State Nominal Values**
Condenser Duty (Q_{cond})	8.6 kW
Reboiler Duty (Q_{reb})	164.5 kw
Buffer Tank Duty (Q_{tank})	155 kW
Outlet valve position of the buffer tank (*V1*)	30 % opening
Outlet valve position of the absorber tank (*V2*)	50 % opening
Outlet valve position of the reboiler tank (*V3*)	50 % opening
Controlled Variables	Set Point
Condenser Temperature (T_{cond})	314 K
Lean Amine temperature (T_{tank})	313 K
Reboiler Temperature (T_{reb})	388.5 K
CO_2 percentage removal %*CC*	95 %
Liquid level in absorber tank (*L2*)	0.3 m
Liquid level in reboiler tank (*L3*)	0.3 m

For the system modelling, the selection of the inputs and the outputs is critical due to taking time in consideration. After the sensitivity analysis and the steady state modelling, the inputs (9) and outputs (8) for the dynamic model were selected as shown in Table 6.

Table 6: Inputs and outputs variables for dynamic modelling.

Variable	Variable Name	Variable Type	Lower Limit	Mid-Point	Upper Limit
x_1	Flow rate of flue gas (mol/s)	Input	3.410625	3.557650869	4.09275
x_2	Temperature of flue gas (K)	Input	312.1968	328.3263415	335.6955
x_3	Pressure of flue gas (kPa)	Input	101.9475	103.7639886	105.0525
x_4	Valve 1 (%)	Input	0.185273	0.209385758	0.265796
x_5	Valve 2 (%)	Input	0.3	0.335149049	0.426142
x_6	Valve 3 (%)	Input	0.3	0.339364177	0.426809
x_7	Condenser Duty (W)	Input	6413.612	7475.737539	9749.903
x_8	Reboiler Duty (W)	Input	96029.92	104513.7614	125995.1
x_9	Tank Duty (W)	Input	86818.87	104370.1245	136342.2
y_1	Liquid Level in absorber sump (m)	Output	0.2957878	0.300034	0.305134
y_2	Reboiler Temperature (K)	Output	388.40985	388.4999	388.6231
y_3	Liquid level in Reboiler sump (m)	Output	0.315427	0.31792	0.320948
y_4	Condenser Temperature (K)	Output	313.0523	315.3805	317.8951
y_5	%CC	Output	88.921165	96.41553	98.81392
y_6	Tank Temperature (K)	Output	307.2121	313.711	322.586
y_7	SER (kJ/kg CO_2)	Output	8846.086	10226.91	11994.63
y_8	Purity	Output	0.841966	0.8984685	0.954971

The open-loop dynamic data was generated by gProms after selecting the proper scenario to guarantee covering all the possible situations where the system variables changes simultaneously. Having 9 input variables manipulated over the lower and upper limit gives a combination of 504 different scenarios, hence, a well schedule of disturbance is needed to ensure the continuous of the simulation and a consistent time and sequence. After about six CPU days, 2632 data points were obtained by recording the input and output variables value each 200 seconds. The simulation was run again with the same setup of scenario and the collected data was compared to make sure it is matching the first run.

The remaining work is determining the best modelling technique for the dynamics, and for this recurrent neural network (*RNN*) are used. The *RNN* are a class of the machine learning modelling techniques where it used to predict and simulate the time dependent processes.

Similar to feedforward neural networks, *RNN* consist of input layer, hidden layer and output layer. The main difference is that *RNN* are trained by the reverse differential mode which means the network has a recurring connection to itself which helps the network to learn the effect of the previous input along with the current or new input.

In *RNN* the connection between components from a supervised cycle is implemented by linking the output of a layer *m* with the input of previous layers < *m* or with its own layer input. This leads to an infeasible system, hence, a real-valued time-delay must be applied to the recurrent links. A Tapped Delay Lines (*TDL*) concept is applied to solve this issue. A *TDL* includes delay operators z^{-d} which delay time-discrete signals by a real-valued delay *d*. Furthermore, the delay elements in a *TDL* are the sets $DI^{l,m}$ and $DL^{l,m}$. All the sets contain real-valued delays d_i between a link from the output of layer *l* to the input of layer *m*. Therefore, for every $d_i \in DI^{l,m}$ or $d_i \in DL^{l,m}$ there has to be a link matrix $IW^{m,l}[d_i]$ or $LW^{m,l}[d_i]$.

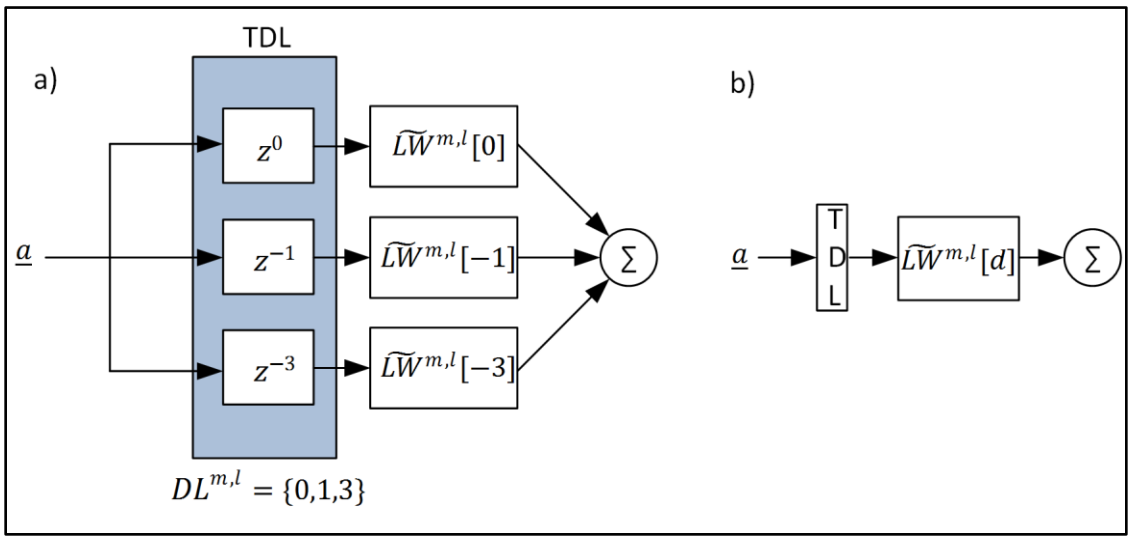

Figure 29: Detailed and simplified tapped delay lines (TDL in pyrenn).

The figure above shows an illustration of *TDL* in a simplified form and detailed one. Three different types of *TDLs* can be introduced to the network, this will add the recursive (time) delayed link with their weight matrices. This effect is illustrated in figure () below. First, for the input delays, $dIn \in [0,1, 2, ...]$, allows to delay the inputs *p* of the *RNN* by a real value time

step $d \geq 0$. The network now can be used for outputs depending on the current input, also the previous input. *dIn* must be non-empty, otherwise no inputs are linked with the neural network. When the existing input is used in the *RNN*, *dIn* must contain 0. Since the delay only affects the inputs, this will not lead to an *RNN* where $DI^{1,1} = dIn$.

Similar to the previous layers, for the output delays $dOut \in [1, 2, ...]$, the recurrent link of the outputs *y* can be added to its first layer. If *dIn* is non-empty, the delays must be greater than 0, $d > 0$ and $DL^{1,M} = dOut$.

Finally, for the internal delays $dIntern \in [1, 2, \ldots]$, the recurrent link is added to all previous layers and to itself except from the output layer. The output layer now depends on the internal state and *dIntern* is non-empty, the delays are greater than zero, therefore, $DL^{m,l} = dIntern \; \forall \; (m \leq l | \; DL^{m,l} \neq DL^{1,M})$.

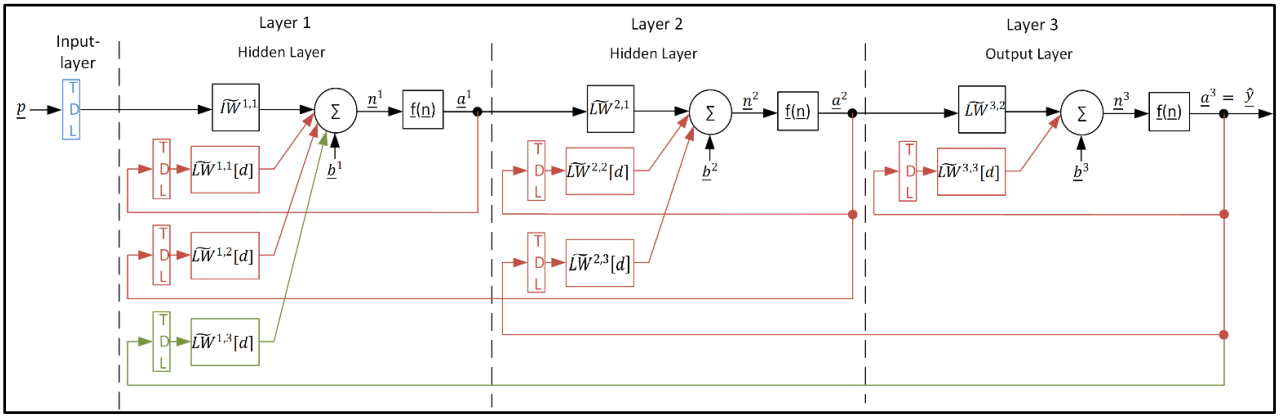

Figure 30: Recurrent connection for a two layers network with possible delays (RNN in pyrenn).

For the training, the *RNN* model, two training algorithms have been used, the Levenberg-Marquardt (*LM*) algorithm and the Broyden-Fletcher-Goldfarn-Shanno algorithm (*BFGS*). The different algorithms are used to minimize the errors in predictions and to reach the best fit of the data. The first training algorithm (*LM*), is known as the damped least squares method which is used to solve and fit non-linear least square problems. The advantage of this algorithm that it interpolates between the Gauss-Newton algorithm (*GNA*) and the method of gradient descent, which means *LM* is more robust than *GNA* and it is capable to find the solution

efficiently even if it is far off the final minimum. However, one disadvantage of *LM* algorithm is finding only local minimum. The second algorithm, *BFGS*, is also a numerical optimization algorithm for solving unconstrained nonlinear problems. The iterative method belongs to the quasi-Newton methods where it seeks a stationary point of a function, hence, a necessary condition for obtaining the optimal solution is that the gradient must be zero. One drawback of *BFGS* that it does not guarantee the fitting of the problem unless the function is a quadratic Taylor expansion near optimum. The *RNN* showed a high performance in predicting the process outputs and was able follow the trends using both training algorithm.

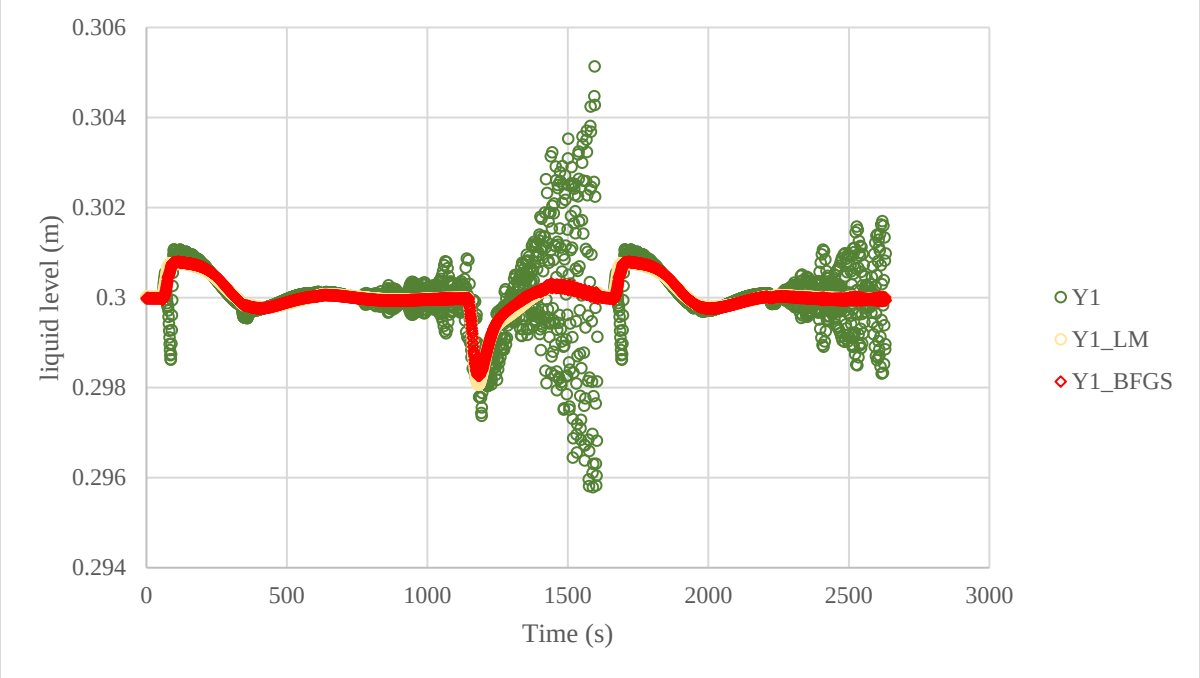

Figure 31: Predicted and measured level of liquid in absorber sump versus time.

The previous plot illustrates the actual liquid level in the absorber sump compared to the predictions using *LM* and *BFGS* algorithms. The *RNN* followed the trend of the original measured data even with the existence of noise. There is some noise in the data presented for the period of t = 1500 s and t = 2500 s. This noise is the result of the controllers trying to keep the liquid level at the set point. The closed-loop control structure is very tight that it caused this behaviour due to the combination of disturbances to the process inputs at the same time.

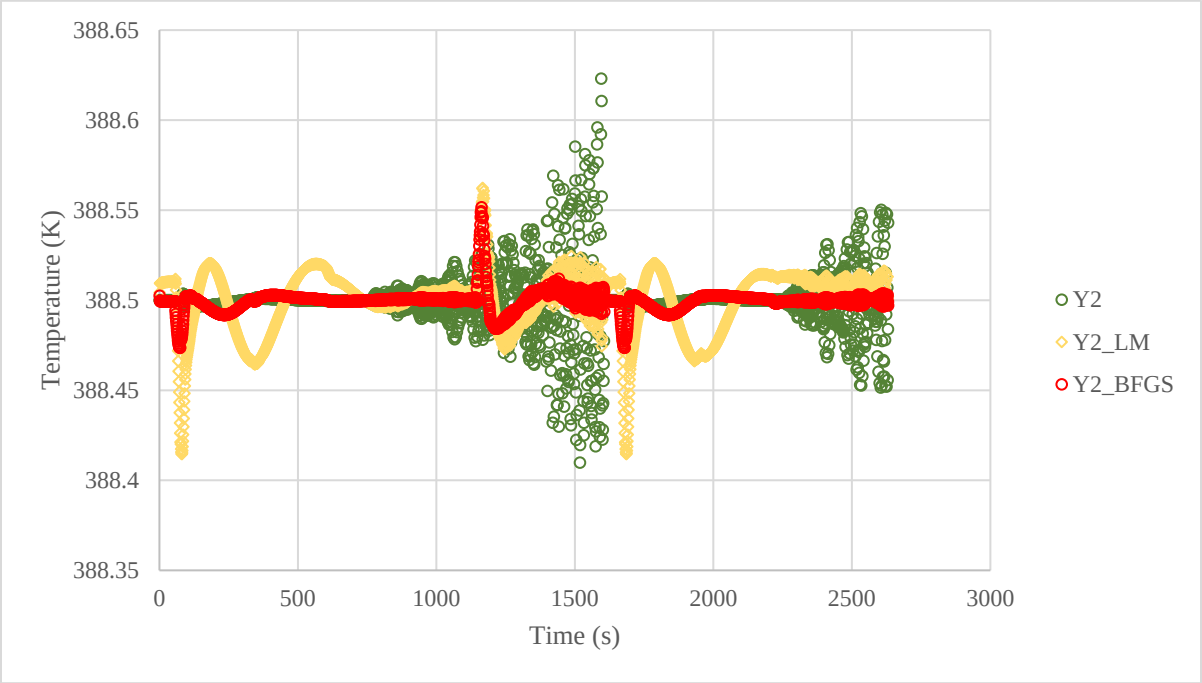

Figure 32: Predicted and measured reboiler temperature.

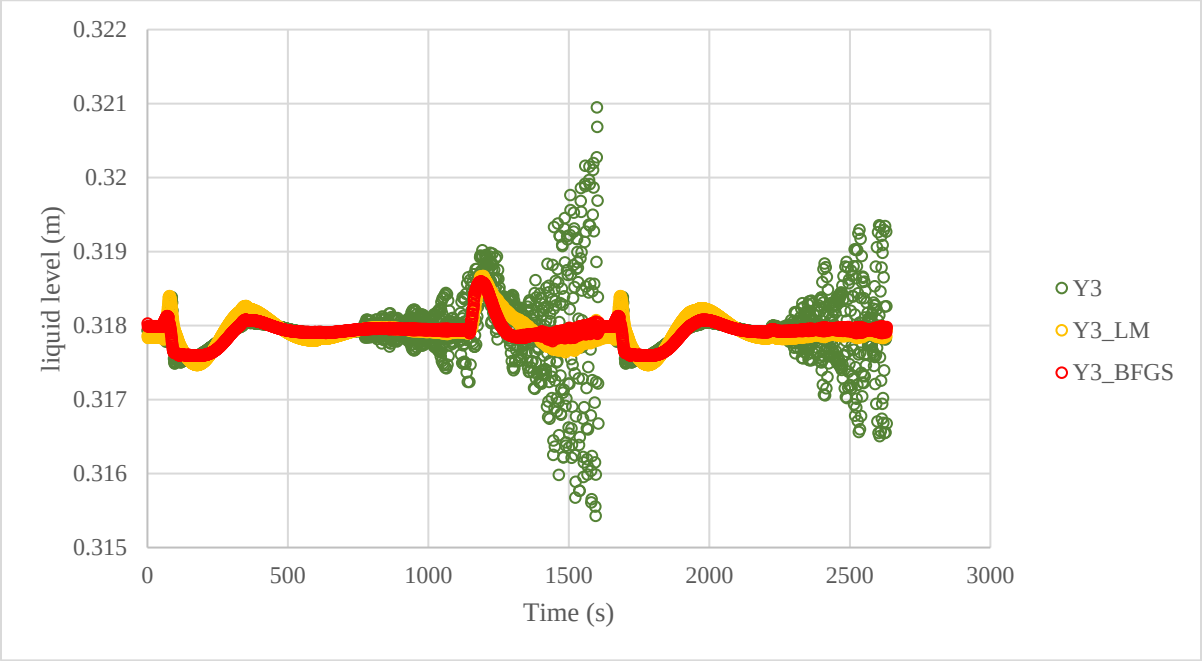

Figure 33: Predicted and measured liquid level in reboiler sump.

For the reboiler temperature and the liquid level in the reboiler surge tank, the same observation is made, however, *BFGS RNN* managed to follow the actual data more precisely.

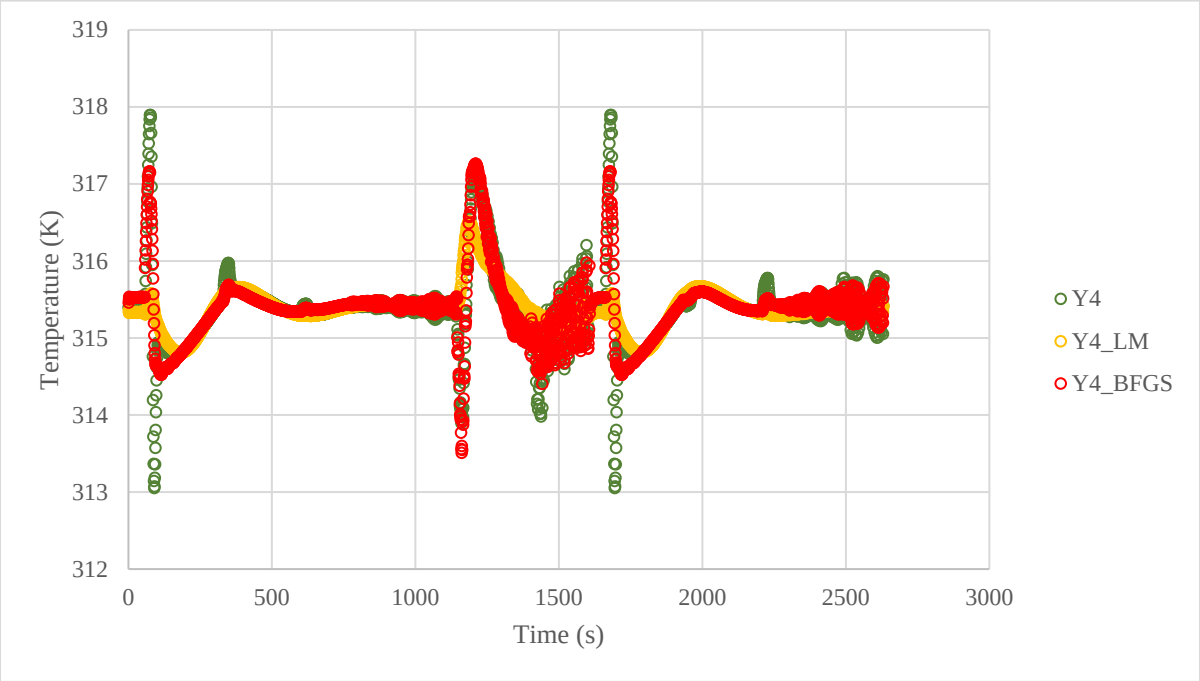

Figure 34: Predicted and measured condenser temperature.

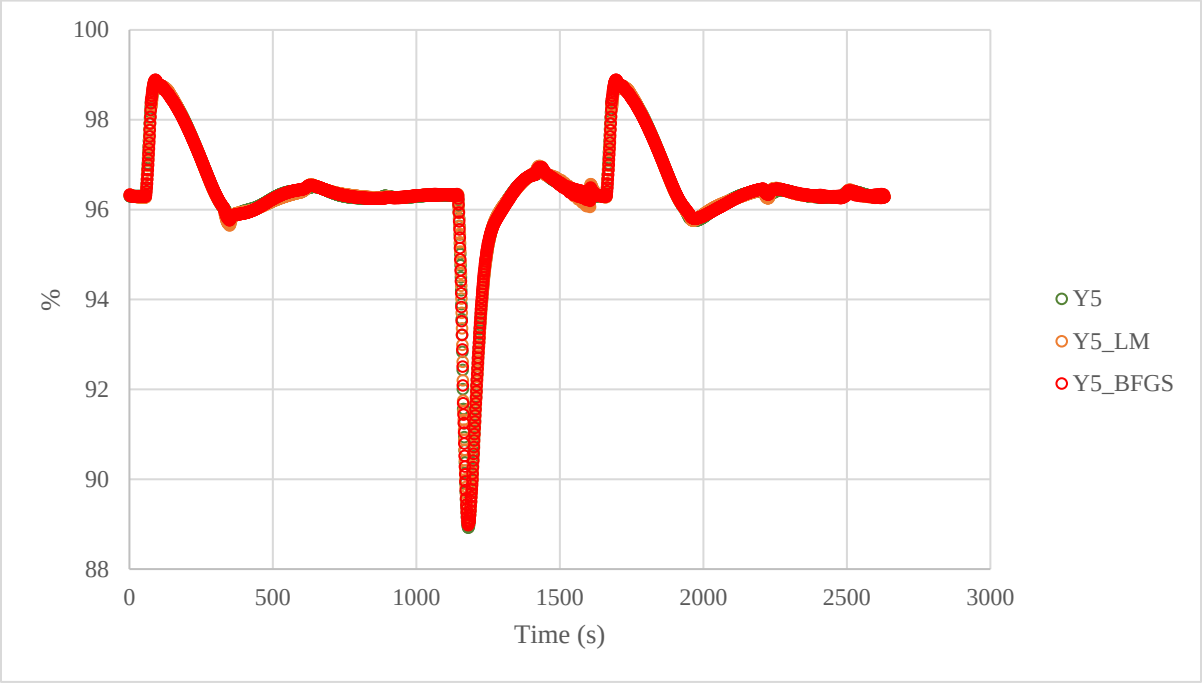

Figure 35: Predicted and measured percentage carbon captured.

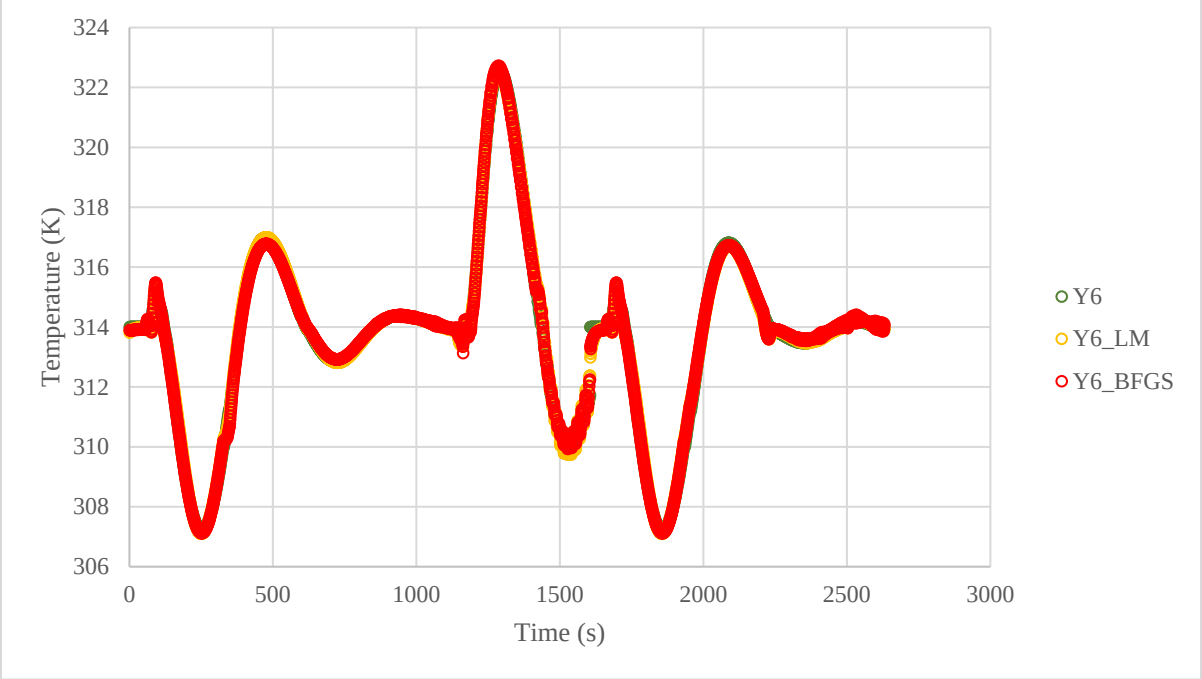

Figure 36: Predicted and measured tank temperature.

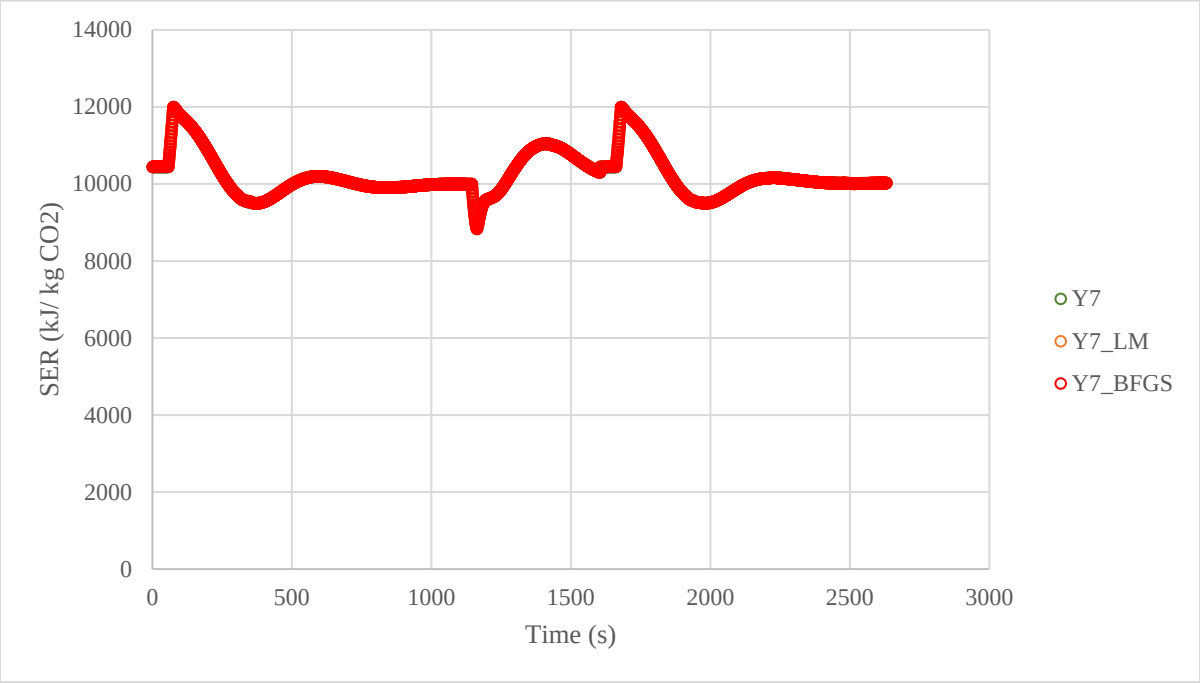

Figure 37: Predicted and measured *SER*.

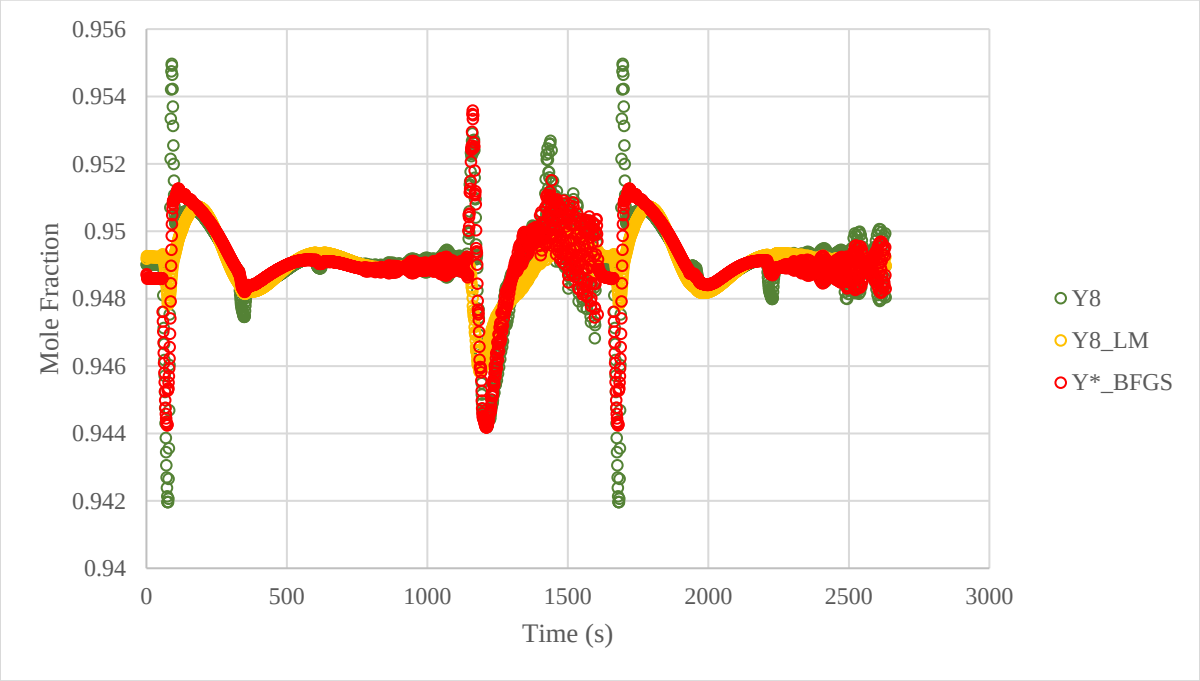

Figure 38: Predicted and measured purity.

For all other outputs, figures (34-38) shows that the *RNN* was able to predict the actual data accurately and the errors were very small. The mean square error (*MSE*) and the regression correlation coefficient (R^2) were calculated. It is illustrated in table (7) that the minimum MSE obtained is 1.785×10^{-7} for liquid level in reboiler sump using *BFGS* training algorithm. The maximum MSE is $2.692 \times {}^{10\text{-}3}$ for the system energy requirement using *LM* algorithm. Moreover, the correlation regression coefficient supported the *MSE* calculation and the maximum R^2 is 0.99847 for the liquid level in reboiler sump using *LM* algorithm, the minimum R^2 is 0.91467 for system energy requirement using *LM* algorithm as well. This proves the credibility of recurrent neural networks to simulate and predict dynamic processes even when the disturbances to the process inputs are occurring simultaneously. The dynamic model can be used later on for model predictive control framework and the tuning of the controllers can be much faster using the *RNN*.

Table 7: Performance evaluation of LM and BFGS RNNs models.

Variable	Mean Square Error	R^2
Liquid level in absorber sump (Y1_LM)	4.95296E-07	0.98792
Liquid level in absorber sump (Y1_BFGS)	4.95128E-07	0.98685
Reboiler Temperature (Y2_LM)	0.000628022	0.92639
Reboiler Temperature (Y2_BFGS)	0.000317141	0.92459
Liquid level in reboiler sump (Y3_LM)	1.79362E-07	0.99847
Liquid level in reboiler sump (Y3_BFGS)	1.78569E-07	0.99264
Condenser Temperature (Y4_LM)	0.000144473	0.94637
Condenser Temperature (Y4_BFGS)	0.00040357	0.93985
%CC (Y5_LM)	2.20291E-05	0.97748
%CC (Y5_BFGS)	1.3237E-05	0.96972
Tank Temperature (Y6_LM)	1.97248E-06	0.98795
Tank Temperature (Y6_BFGS)	1.89199E-05	0.98673
SER (Y7_LM)	2.69E-03	0.91467
SER (Y7_BFGS)	1.23E-04	0.93967
Purity (Y8_LM)	1.01995E-06	0.97878
Purity (Y8_BFGS)	2.87411E-07	0.98119

Chapter 4: Optimization

In this section, optimization of the process operating conditions is discussed. The goal of the optimization from operational point of view is to reduce and minimize the energy consumed by the reboiler, mainly, and the condenser and the makeup tank. Moreover, it is required to increase the capturing rate and the purity of carbon dioxide as the final product of the process. The formulation of the objective function will determine how and what are the best algorithms to be used to solve the problem. Two optimization algorithms are used in this work to provide optimal solutions/ optimal operating conditions.

4.1 Sequential Quadratic Programming

After developing and testing the different modes, it was concluded that the *ANN* model gives the best results in predictions and performance compared to the other models. It is essential to use it to determine the optimum operating condition of the *PCC* unit alongside with the model as a prediction tool. The *ANN* will replace the model equations or process data and optimization will be done in a high-speed processing (Elkamel, 1998). It is clear since the developed *ANN* model consists of 9 variables that a non-linear problem (*NLP*) problem will rise. In general, operational objectives would include reducing the system requirements (*SER*), increasing the capture rate (*CR*) and the purity of CO_2 at the condenser outlet stream (*PU*). A possible objective function combining all three objectives (minimizing *SER,* maximizing *CR* and maximizing *PU*) thereby testing the *ANN's* ability in performing multi-objective optimization. This multi-objective function can be written as follows:

$$minimize\ f(x) = \left[\frac{\mathrm{SER}(x)}{\mathrm{SER}^{\mathrm{U}}} - \frac{\mathrm{PU}(x)}{\mathrm{PU}^{\mathrm{U}}} - \frac{\mathrm{CR}(x)}{\mathrm{CR}^{\mathrm{U}}}\right] \tag{9}$$

$$\text{s. t.} \qquad g_i\,(x) = 0 \qquad i = 1, 2 \ldots M \tag{10}$$

$$g_i\,(x) \leq 0 \qquad i = M + 1, 2 \ldots N \tag{11}$$

where *x* is the vector inputs variables to the *ANN* model. The function *f* (*x)* is evaluated first by evaluating each output *SER*, *PU* and *CR* at each input vector using the developed *ANN* then the function is calculated according to equation (9). The equality and inequality constraints of the model is shown by equation (10) and (11). When the manipulation of all inputs variables is not possible the equality constraints are used. On the other hand, inequality constraints are used when the upper and lower bounds of the variables are available. The variables in equation (9) are scaled and made dimensionless by dividing them by their upper limit so their values range between 0 and 1. To obtain the solution, constraints must be added to the problem (Elkamel, 1998; Li et al., 2013). For example, the upper and lower limits on the variables are used to obtain a solution within the trained data set. This problem is solved using a sequential quadratic programming algorithm by (Gill, Murray, Saunders, & Wright, 1984). The main idea is to formulate a sub problem based on the quadratic approximation of the Lagrangian L(x, λ) = $f(x)$ +$\sum_{i=1}^{N} \lambda_i g_i(x)$, and for iteration *k* can be presented as

$$\text{Minimize } \frac{1}{2} d_k^T H_k d_k + \nabla f(x_k)^T d_k \tag{12}$$

$$\nabla g_i(x_k)^T d_k + g_i(x_k) = 0 \qquad i = 1, \ldots\ldots, M \tag{13}$$

$$\nabla g_i(x_k)^T d_k + g_i(x_k) \leq 0 \qquad i = \mathrm{M}+1, \ldots\ldots, N \tag{14}$$

Where H_k is a positive matrix approximating the Hessian matrix at iteration *k* of the Lagrangian function and d_k is the direction of search. The sub problem is solved by producing a vector d_k to calculate new iteration x_{k+1}($x_{k+1} = x_k + \alpha_k d_k$). while the Hessian matrix is updated by

$$H_{kH} = H_k + \frac{q_k q_k^T}{q_k^T s_k} - \frac{H_k^T H_k}{s_k^T H_k s_k} \tag{15}$$

Where

$$s_k = x_{k+1} - x_k \tag{16}$$

$$q_k = \nabla f\ (x_{k+1}) + \sum_{i=1}^{N} \lambda_i \nabla g_i(x)_{k+1} - \left(\nabla f(x_k + \sum_{i=1}^{N} \lambda_i \nabla g_i(x)_k \right) \tag{17}$$

4.2 Genetic Algorithm

Another optimisation method to be tested is that of genetic algorithms (*GA*). Although both the *SQP* and *GA* methods are not guaranteed to provide global solutions, the *GA* might provide a better solution than the one obtained by *SQP*. *GA* is an inspired algorithm based on genetics and natural selection introduced by (Goldberg & Holland, 1988). The algorithm simply works by searching over the population which consists a number of solutions. Every single solution represents a chromosome with set of genes which makes it unique. Initially, a fitness function is used to select the best solutions.

Then, a mating process between solutions starts to provide higher quality solutions. The first generation during the mating process are called the parents. (Koza, Hall, & Holland, 1995) explained that every parent will generate two children and it is expected that the offspring will have better quality than the parents. The better solutions will eliminate the earlier ones and the process repeats until the optimal solution is reached. However, a replacement process is needed to overcome the drawback of the possibility to generate some parents from the offspring. Where the old population is being replaced by a new one to assure the generation of a new and better solutions every time. The mating process can be applied by to variations, crossover and mutation. In crossover, the selection of genes to be given to the offspring is random from the parents (Koza et al., 1995).

On the other hand, in mutation, some genes in the offspring are selected and changed to provide uniqueness to the solution. In this work, *GA* was applied on the same objective function introduced in the previous section. The algorithm was implemented in MATLAB where the population size is determined to be 200 since 9 variables are being studied. The selection is done by tournament process where individuals are selected randomly. The crossover fraction is varied from 0 to 1 to guarantee the generation of unique offspring over a wide range.

Later on, the mutation function is Gaussian to add a random number to each vector f individual entry. Additional migration process is used with a forward direction to provide the movements between sub-populations, so the best solutions eliminates the undesired ones. The algorithm

will give the optimal solution after the stopping criteria is met. The stopping criteria is set to be the number of generations where the program stops after generating 900 generations.

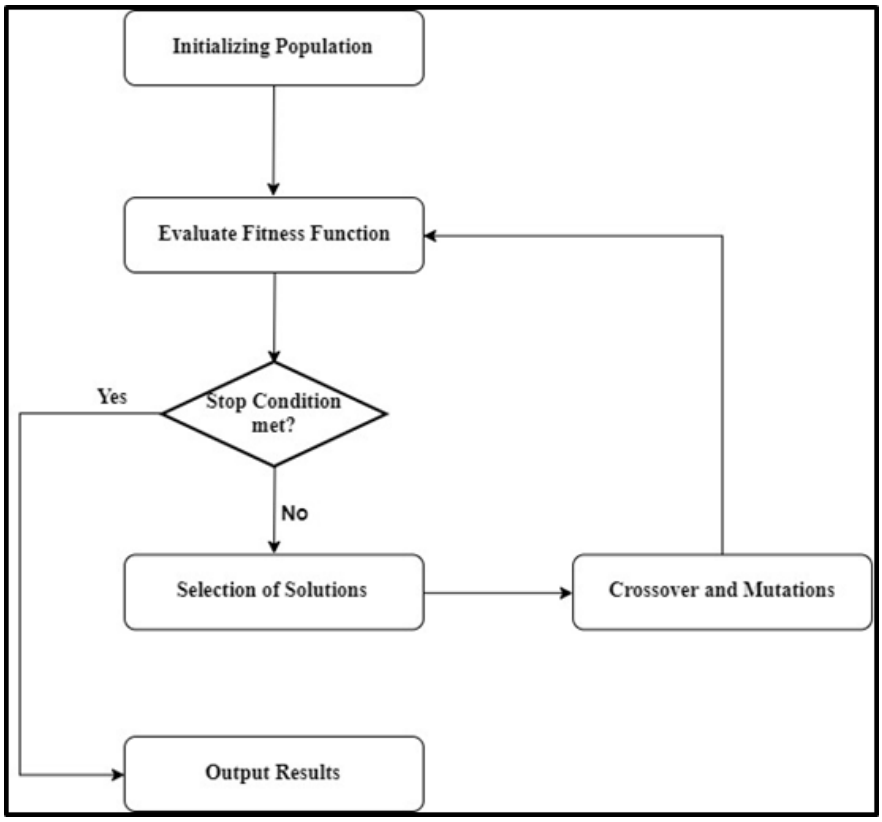

Figure 39: Genetic algorithm mechanism.

Imposing the lower and upper limits on the variables given in Table.1 the optimization problem was solved. The optimal operating conditions, the value of the outputs and the objective function value are summarized in table (8) below.

Table 8: Optimization Summary.

Variables	Nominal Operation	Optimal Results				
		Min. equation (9)		Min. SER only	Max. PU only	Max. CR only
		SQP	GA	SQP	SQP	SQP
Flow Rate (mol/s)	4.0125	5.128	3.21^{l}	5.128^{u}	5.128^{u}	3.222
Temperature (K)	319.71	300.236	308.459	317.943	299.003	310.082
Pressure (kPa)	103.5	106.57	110^{u}	109.99	109.98	96.37
Reboiler Pressure (kPa)	160	179.99	162.98	179.90	180^{u}	143.94
Reboiler Duty (W)	153,600	16,2108.39	150,228.10	170,000	150,000	150,000
Condenser Duty (W)	8,600	7,177.084	8,039.959	6,600	7,000.154	7,000
SER (kJ/kg CO_2)	11,324.16	10,415.93	14,936.41	8,851.71	11,054.82	15,684.17
PU	0.938	0.976	0.918	0.835	0.969	0.912
CR (%)	96.360	97.073	99.696	92.762	72.119	99.981
Objective Function	-1.8511	-1.3393	-1.5582	0.5415	-0.9696	-1

^{l} = lower limit, ^{u} = upper limit

The third column represents the solution obtained after applying the *SQP* algorithm over the objective function in equation (9). The solution recommends using the maximum flow rate for the flue gas and the upper limit of the flue gas pressure to obtain 97% capturing rate and a total energy requirement of 10415.926 kJ/kg CO_2. On the fourth column the same objective function is solved using *GA* and the solution recommends using the lower limit of the flue gas flow rate with the maximum pressure to obtain 99.7% capturing rate and total energy requirement of 14936.41 kJ/kg CO_2.

The objective function value obtained by *SQP* was higher than the one obtained by *GA*, however, from an engineering point of view, *SQP* represents the better solution as minimum energy is required and a satisfying capturing rate and purity is achieved at the same time.

Furthermore, the optimization was performed over each output alone to study the possibility of achieving satisfying operating conditions. The fifth column represents the optimal operating points for the minimization of *SER* only. Only 8,851 kJ/kg CO_2 is required when the flow rate of flue gas is at the maximum. Also, maintaining the flue gas feed at a high pressure and temperature results in a 92% capturing rate. However, the required condenser duty is at the lower limit which explains the purity of 0.83 for the CO_2 coming as the product.

In the sixth column, the optimization goal was to maximize the purity of carbon dioxide only. From the results, it is clear that this solution is not feasible as the maximum purity was not achieved and the capturing rate is 72% which is below the acceptable limits. Finally, in the last column, maximizing the capturing rate was the goal of the optimization and satisfying results has been obtained. Almost 100% capturing rate is achieved with a purity of 0.91 but higher *SER* is obtained than all other cases. The recommended optimization algorithm as it provided the best solution over other cases is to use *SQP* over the objective function presented by equation (9).

Chapter 5: Conclusion & Recommendations

The objective of this research was to model a post combustion CO_2 capturing unit using machine learning regression techniques, and to use the surrogated models to optimize the operational process inputs to minimize the overall energy consumption and maximize the capturing rate and the purity of carbon dioxide. This work consisted of four major steps which are, a) post combustion capturing unit developed by (Nittaya, 2014) and sensitivity analysis to study the effect of disturbances to system inputs on the outputs. Furthermore, b) generation of data using gProms v.5.1 for both steady state and dynamic modelling. Next, c) using different machine learning techniques such as artificial neural network (*ANN*) and Gaussian Process Regression (*GPR*) for steady state modelling. Multiple disturbances were introduced simultaneously to the system inputs to generate more than 300 data point for modelling. The *ANN* excelled all other developed models in predicting the process outputs with an accuracy of 98%.

For dynamic modelling, 2632 data points were generated after introducing disturbances to the system inputs and adding more variables to be observed and predicted since controllers are activated. Recurrent neural networks (*RNN*) were used to predict the system outputs and study the dynamic behaviour of the post combustion unit. Two different training algorithms were used, *LM* and *BFGS* in building the *RNN* and high performance in predicting all the system outputs was obtained. A minimum of 91% accuracy was achieved in predicting the system energy requirement using *LM* algorithm. A maximum accuracy of 98.7% in predicting liquid level in the absorber sump using *LM* algorithm which was slightly higher than *BFGS*.

Finally, optimization of the process operating conditions was performed using two different methods, sequential quadratic programming (*SQP*) and genetic algorithm (*GA*). The ANN was optimized to minimize the normalized system energy requirement (SER) minus the normalized capture rate minus the normalized carbon dioxide purity in the outlet stream. The objective function value using the *GA* was -1.5582, which is better than -1.3393 (the value obtained

when using *SQP*). However, the results using *SQP* were judged to be better since the *SER* was 30% lower compared to the value obtained using the *GA*. Furthermore, both optimization methods resulted in local optimal solutions since the upper and lower limits were used to constraint the problem and imposing more constraints to the problem would lead to a better solution.

Future work should continue exploring alternative machine learning approaches to model the system and to increase the accuracy of the prediction by using more operational historical data. Moreover, combining the close-loop to the developed *RNN* as it is suggested to use the *RNN* in programming and setting the controllers of the system to manage dealing with the disturbance faster and overcome the delays. It is also recommended to apply the theoretical knowledge in this work on a pilot scale plant to test the validity of the developed models. Using different input variables and different optimization algorithms is proposed to obtain better optimal operating conditions (global), and more data will enhance the performance of the developed model in terms of accuracy and error reduction.

References

Ahmad, F. (2019). *Dynamic Scheduling and Control of MEA Absorption Processes for CO2 Capture Using gProms*. University of Waterloo. Retrieved from http://hdl.handle.net/10012/14788

Al-Shayaji, K., Al-Wadyei, S., & Elkamel, A. (2006). Modelling and optimization of a multistage flash desalination process. *Engineering Optimization*, *37*(6), 591–607. https://doi.org/10.1080/03052150412331335801

Allam, R. J., Palmer, M. R., Brown, G. W., Fetvedt, J., Nomoto, H., Itoh, M., … Jones, C. (2013). High efficiency and low cost of electricity generation from fossil fuels while eliminating atmospheric emissions , including carbon dioxide. *Energy Procedia*, *37*, 1135–1149. https://doi.org/10.1016/j.egypro.2013.05.211

Babu, P., Wen, H., Ong, N., & Linga, P. (2016). A systematic kinetic study to evaluate the effect of tetrahydrofuran on the clathrate process for pre-combustion capture of carbon dioxide. *Energy*, *94*, 431–442. https://doi.org/10.1016/j.energy.2015.11.009

Bae, T., Hudson, M. R., Mason, J. A., Queen, W. L., Dutton, J. J., Sumida, K., … Long, R. (2013). Environmental Science post-combustion carbon dioxide capture. *Energy Environ.Sci*, (6), 128–138. https://doi.org/10.1039/c2ee23337a

Behbahani, R. M., Jazayeri-rad, H., & Hajmirzaee, S. (2009). Fault Detection and Diagnosis in a Sour Gas Absorption Column Using Neural Networks, (5), 840–845. https://doi.org/10.1002/ceat.200800486

Bishoyi, D., & Sudhakar, K. (2017). Modeling and performance simulation of 100MW PTC based solar thermal power plant in Udaipur India. *Case Studies in Thermal Engineering*, *10*, 216–226. https://doi.org/10.1016/j.csite.2017.05.005

Brettschneider, O., Thiele, R., Faber, R., Thielert, H., & Wozny, G. (2004). Experimental investigation and simulation of the chemical absorption in a packed column for the system NH3 – CO2 – H2S – NaOH – H2O. *Separation and Purification Technology*, *39*, 139–159. https://doi.org/10.1016/S1383-5866(03)00165-5

Casas, N., Schell, J., Joss, L., & Mazzotti, M. (2013). A parametric study of a PSA process for pre-combustion CO2 capture. *Separation and Purification Technology*, *104*, 183–192. https://doi.org/10.1016/j.seppur.2012.11.018

Chan, V., & Chan, C. (2017). Learning from a carbon dioxide capture system dataset : Application of the piecewise neural network algorithm. *Petroleum*, *3*(1), 56–67. https://doi.org/10.1016/j.petlm.2016.11.004

Chatterjee, A. (2000). An introduction to the proper orthogonal decomposition. *Current Science*, *78*(7), 808–817.

Chen, L., Yong, S. Z., & Ghoniem, A. F. (2012). Oxy-fuel combustion of pulverized coal : Characterization , fundamentals , stabilization and CFD modeling. *Progress in Energy and Combustion Science*, *38*(2), 156–214. https://doi.org/10.1016/j.pecs.2011.09.003

Dai, Z., & Deng, L. (2016). Membrane absorption using ionic liquid for pre-combustion CO2 capture at elevated pressure and temperature. *International Journal of Greenhouse Gas Control*, *54*, 59–69. https://doi.org/10.1016/j.ijggc.2016.09.001

Draper, A. M., & Weissburg, M. J. (2019). Impacts of Global Warming and Elevated CO2 on

Sensory Behavior in Predator-Prey Interactions : A Review and Synthesis. *Frontiers in Ecology and Evolution*, *7*(March), 19. https://doi.org/10.3389/fevo.2019.00072

Elbatran, A., Yaakob, O., Ahmed, Y. M., & Ismail, M. A. (2015). Hydro Power and Turbine Systems Reviews. *Jurnal Teknologi*, (May). https://doi.org/10.11113/jt.v74.4646

Elkamel, A. (1998). An artificial neural network for predicting and optimizing immiscible flood performance in heterogeneous reservoirs. *Computers and Chemical Engineering*, *22*(11).

Environ, E., Mason, J. A., Sumida, K., Herm, Z. R., & Long, J. R. (2011). Environmental Science Evaluating metal – organic frameworks for post-combustion carbon dioxide capture via temperature swing adsorption †, 3030–3040. https://doi.org/10.1039/c1ee01720a

García, S., Gil, M. V, Martín, C. F., Pis, J. J., Rubiera, F., & Pevida, C. (2011). Breakthrough adsorption study of a commercial activated carbon for pre-combustion CO2 capture, *171*, 549–556. https://doi.org/10.1016/j.cej.2011.04.027

Ghiasi, M. M., Abedi-farizhendi, S., & Mohammadi, A. H. (2019). Modeling Equilibrium Systems of Amine-Based CO2 Capture by Implementing Machine Learning Approaches. *Environmental Progress and Sustainable Energy*, *38*(5), 1–12. https://doi.org/10.1002/ep.13160

Gill, P. E., Murray, W., Saunders, M. A., & Wright, M. H. (1984). Procedures for Optimization Problems with a Mixture of Bounds and General Linear Constraints, *10*(3), 282–298.

Goldberg, D., & Holland, J. (1988). Genetic Algorithms and Machine Learning, 95–99.

Hansen, J., Ruedy, R., Sato, M., & Lo, K. (2010). GLOBAL SURFACE TEMPERATURE CHANGE. *Reviews of Geophysics*, *48*, 1–29. https://doi.org/10.1029/2010RG000345.

Harun, N. (2012). *Dynamic Simulation of MEA Absorption Process for CO2 Capture from Power Plants*. University of Waterloo. Retrieved from http://hdl.handle.net/10012/6564

Ho, S., Jong, S., Wook, J., Nam, S., & Bin, J. (2014). The quantitative evaluation of two-stage pre-combustion CO2 capture processes using the physical solvents with various design parameters. *Energy*, 1–9. https://doi.org/10.1016/j.energy.2014.10.055

Jacobson, M. Z. (2009). Review of solutions to global warming , air pollution , and energy security †, 148–173. https://doi.org/10.1039/b809990c

Jiang, G., Huang, Q., Danaei, S., Hu, X., Russell, A. G., Fan, M., & Shen, X. (2015). A new mesoporous amine-TiO2 based pre-combustion CO2 capture technology. *Applied Energy*, *147*, 214–223. https://doi.org/10.1016/j.apenergy.2015.01.081

Koroglu, B., Pryor, O. M., Lopez, J., Nash, L., & Vasu, S. S. (2016). Shock tube ignition delay times and methane time-histories measurements during excess CO2 diluted oxy-methane combustion. *Combustion and Flame*, *164*, 152–163. https://doi.org/10.1016/j.combustflame.2015.11.011

Koza, J. R., Hall, M. J., & Holland, J. (1995). Survey of genetic algorithms and genetic programming. In *Wescon conference record* (pp. 589–594).

Kramer, M. A. (1991). Nonlinear Principal Component Analysis Using Autoassociative Neural Networks, *37*(2), 233–243.

Lawal, A., Wang, M., Stephenson, P., & Yeung, H. (2009). Dynamic modelling of CO2 absorption for post combustion capture in coal-fired power plants. *Fuel*, *88*(12), 2455–2462. https://doi.org/10.1016/j.fuel.2008.11.009

Lee, J. H., & Min, J. (2006). Approximate dynamic programming based approach to process control and scheduling, *30*, 1603–1618. https://doi.org/10.1016/j.compchemeng.2006.05.043

Lee, J. H., Shin, J., & Realff, M. J. (2018). Machine learning : Overview of the recent progresses and implications for the process systems engineering field. *Computers and Chemical Engineering*, *114*, 111–121. https://doi.org/10.1016/j.compchemeng.2017.10.008

Lee, Z. H., Lee, K. T., Bhatia, S., & Mohamed, A. R. (2012). Post-combustion carbon dioxide capture : Evolution towards utilization of nanomaterials. *Renewable and Sustainable Energy Reviews*, *16*(5), 2599–2609. https://doi.org/10.1016/j.rser.2012.01.077

Li, Z., Sharma, M., Khalilpour, R., & Abbas, A. (2013). Optimal Operation of Solvent-based Post-combustion Carbon Capture Processes with Reduced Models. *Energy Procedia*, *37*, 1500–1508. https://doi.org/10.1016/j.egypro.2013.06.025

Liu, G. B., Yu, K. T., Yuan, X. G., Liu, C. J., & Guo, Q. C. (2006). Simulations of chemical absorption in pilot-scale and industrial-scale packed columns by computational mass transfer, *61*, 6511–6529. https://doi.org/10.1016/j.ces.2006.05.035

Martin, C. F., Stockel, E., Clowes, R., J. Adams, D., I.Cooper, A., Pis, J. J., … Pevida, C. (2011). Hypercrosslinked organic polymer networks as potential adsorbents for pre-combustion CO2 capture. *Journal of Materials Chemicstry*, *21*, 5475–5483. https://doi.org/10.1039/c0jm03534c

Mazas, A., Lacoste, D., & Schuller, T. (2016). Experimental and numerical investigation on the laminar flame speed of CH4 / O2 mixtures diluted with CO2 and H2O. *ASME*.

Merkel, T. C., Lin, H., Wei, X., & Baker, R. (2010). Power plant post-combustion carbon dioxide capture : An opportunity for membranes. *Journal of Membrane Science*, *359*(1–2), 126–139. https://doi.org/10.1016/j.memsci.2009.10.041

Moioli, S., Giuffrida, A., Gamba, S., Romano, M. C., Pellegrini, L., & Lozza, G. (2014). Pre-combustion CO2 capture by MDEA process in IGCC based on air-blown gasification. *Energy Procedia*, *63*(December), 2045–2053. https://doi.org/10.1016/j.egypro.2014.11.220

Nittaya, T. (2014). *Dynamic Modelling and Control of MEA Absorption Processes for CO2 Capture from Power Plants*. Retrieved from http://hdl.handle.net/10012/8128

Nittaya, T., Douglas, P. L., Croiset, E., & Ricardez-sandoval, L. A. (2014). Dynamic Modelling and Controllability Studies of a Commercial-scale MEA Absorption Processes for CO2 Capture from Coal-fired Power Plants ScienceDirect Dynamic Modelling and Controllability Studies of a Commercial- Scale MEA Absorption Processes for CO2. *Energy Procedia*, *63*, 1595–1600. https://doi.org/10.1016/j.egypro.2014.11.169

Oh, J., & Noh, D. (2012). Laminar burning velocity of oxy-methane fl ames in atmospheric condition. *Energy*, *45*(1), 669–675. https://doi.org/10.1016/j.energy.2012.07.027

Poompavai, T., & Kowsalya, M. (2019). Control and energy management strategies applied for solar photovoltaic and wind energy fed water pumping system : A review. *Renewable and Sustainable Energy Reviews*, *107*(November 2018), 108–122. https://doi.org/10.1016/j.rser.2019.02.023

Pryor, O., Barak, S., Lopez, J., Ninnemann, E., Koroglu, B., Nash, L., & Vasu, S. (2017). High presure shock tube ignition delay time measurements during oxy-methane combustion with high levels of co2 dilution. *Energy Resources Technology*, *139*(4). https://doi.org/10.1115/1.4036254

Ranisau, J., Barbouti, M., Trainor, A., Juthani, N., Salkuyeh, Y. K., Maroufmashat, A., & Fowler, M.

(2017). Power-to-gas implementation for a polygeneration system in southwestern ontario. *Sustainability (Switzerland)*, *9*(9). https://doi.org/10.3390/su9091610

Raza, A., Gholami, R., Rezaee, R., Rasouli, V., & Rabiei, M. (2019). Significant aspects of carbon capture and storage – A review. *Petroleum*, *5*(4), 335–340. https://doi.org/10.1016/j.petlm.2018.12.007

Romano, M. C., Chiesa, P., & Lozza, G. (2010). International Journal of Greenhouse Gas Control Pre-combustion CO2 capture from natural gas power plants , with ATR and MDEA processes. *International Journal of Greenhouse Gas Control*, *4*(5), 785–797. https://doi.org/10.1016/j.ijggc.2010.04.015

Said, A., Eloneva, S., Fogelholm, C., & Fagerlund, J. (2011). Energy Procedia Integrated carbon capture and storage for an oxyfuel combustion process by using carbonation of Mg(OH)2 produced from serpentinite rock. *Energy Procedia*, *4*, 2839–2846. https://doi.org/10.1016/j.egypro.2011.02.189

Saifullah, A. Z. A., Karim, A., & Karim, R. (2016). Wind Energy Potential in Bangladesh. *American Journal of Engineering Research (AJER)*, *5*(7), 85–94.

Savile, C. K., & Lalonde, J. J. (2011). Biotechnology for the acceleration of carbon dioxide capture and sequestration. *Current Opinion in Biotechnology*, *22*(6), 818–823. https://doi.org/10.1016/j.copbio.2011.06.006

Schell, J., Casas, N., Blom, R., Spjelkavik, A. I., Andersen, A., Hafizovic, J., & Marco, C. (2012). MCM-41, MOF and UiO-67/MCM-41 adsorbents for pre-combustion CO2 capture by PSA : adsorption equilibria. *Adsorption*, (18), 213–227. https://doi.org/10.1007/s10450-012-9395-1

Scholes, C. A., Ho, M. T., Wiley, D. E., Stevens, G. W., & Kentish, S. E. (2013). International Journal of Greenhouse Gas Control Cost competitive membrane — cryogenic post-combustion carbon capture. *International Journal of Greenhouse Gas Control*, *17*, 341–348. https://doi.org/10.1016/j.ijggc.2013.05.017

Seeger, M. (2004). Gaussian Processes for Machine Learning. *International Journal of Neural Systems*, *14*(2), 69–106. https://doi.org/https://doi.org/10.1142/S0129065704001899

Shahsavand, A., Fard, F. D., & Sotoudeh, F. (2011). Application of arti fi cial neural networks for simulation of experimental CO2 absorption data in a packed column. *Journal of Natural Gas Science and Engineering*, *3*(3), 518–529. https://doi.org/10.1016/j.jngse.2011.05.001

Shin, J., Lee, J. H., & Realff, M. J. (2017). Operational planning and optimal sizing of microgrid considering multi-scale wind uncertainty. *Applied Energy*, *195*, 616–633. https://doi.org/10.1016/j.apenergy.2017.03.081

Sifat, N. S., & Haseli, Y. (2019). A Critical Review of CO2 Capture Technologies and Prospects for Clean Power Generation. *Energies*, *12*(21). https://doi.org/https://doi.org/10.3390/en12214143

Stanger, R., & Wall, T. (2011). Sulphur impacts during pulverised coal combustion in oxy-fuel technology for carbon capture and storage. *Progress in Energy and Combustion Science*, *37*(1), 69–88. https://doi.org/10.1016/j.pecs.2010.04.001

Wappel, D., Gronald, G., Kalb, R., & Draxler, J. (2010). International Journal of Greenhouse Gas Control Ionic liquids for post-combustion CO2 absorption. *International Journal of Greenhouse Gas Control*, *4*(3), 486–494. https://doi.org/10.1016/j.ijggc.2009.11.012

Xie, Y., Wang, J., Zhang, M., Gong, J., Jin, W., & Huang, Z. (2013). Experimental and Numerical Study on Laminar Flame Characteristics of Methane Oxy-fuel Mixtures Highly Diluted with CO2. *Energy Fuels*, *27*(10), 6231–6237.

Yang, M., Jing, W., Zhao, J., Ling, Z., & Song, Y. (2016). Promotion of hydrate-based CO2 capture from flue gas by additive mixtures (THF(tetrahydrofuran) + TBAB (tetra-n-butyl ammonium bromide)). *Energy*, *106*, 546–553. https://doi.org/10.1016/j.energy.2016.03.092

Zheng, J., Zhang, P., & Linga, P. (2016). Semiclathrate hydrate process for pre-combustion capture of CO2 at near ambient temperatures. *Applied Energy*, *194*, 267–278. https://doi.org/10.1016/j.apenergy.2016.10.118

Appendix A

Steady state sensitivity analysis.

Flue gas flow rate	SER	%CC	PU
3.009375	13266.96	99.28634	0.8921754
3.289414	12153.4	98.99757	0.9198547
3.569453	11226.56	98.61866	0.925988
3.849492	10447.68	98.14462	0.9418405
4.129531	9789.823	97.55303	0.9528117
4.40957	9237.581	96.77143	0.9612555
4.68961	8787.341	95.65035	0.9692125
4.969648	8446.363	93.96826	0.9751409
5.025656	8392.624	93.54128	0.9848458

Flue gas pressure	SER	%CC	PU
90.5625	12698.114	89.3274	0.948375
91.65931	12179.596	90.0397	0.943375
92.75613	11679.473	90.7631	0.938375
93.852936	11379.2384	91.4861	0.932953
94.94975	11078.6714	92.0984	0.927530
96.04656	10777.6914	92.7218	0.922108
97.14337	10477.5674	93.3205	0.916685
98.24019	10327.3334	93.8748	0.910248
99.337	10177.2104	94.3859	0.903811
100.433815	10027.0874	94.8846	0.897374
101.530624	9876.96444	95.35	0.890937
102.62743	9726.84144	95.7932	0.884500
103.72425	9576.71844	96.1919	0.878063
104.82106	9426.59544	96.5684	0.871626
105.91788	9276.47244	96.9005	0.865189
107.01469	9126.34944	97.1992	0.858752
108.1115	8976.22644	97.4757	0.852315
109.20831	8826.10344	97.6878	0.845878
110.30512	8675.98044	97.8999	0.839441

Flue gas Temperature	SER	%CC	PU
298.92886	10437.6	96.28846	0.9493259
301.20404	10438.1	96.16506	0.9463259
303.47922	10438.66	96.04166	0.9433259
305.7544	10439.58	95.82866	0.9403259
308.02957	10440.8	95.61566	0.9373259
310.30475	10442.28	95.40266	0.9351859
312.57993	10443.99	95.18966	0.9330459
314.8551	10445.91	94.97666	0.9309059
317.1303	10448.01	94.76366	0.9289189
319.4055	10450.24	94.55066	0.9269319
321.68066	10452.48	94.33766	0.9249449
323.95584	10454.7	94.12466	0.9213849
326.23102	10456.89	93.82266	0.9178249
328.5062	10459.01	93.52066	0.9142649
330.78137	10461.08	93.21866	0.9107049
333.05655	10463.09	92.91666	0.9071449
335.33173	10465.03	92.61466	0.8992449
337.60693	10466.92	92.31266	0.8913449
339.8821	10468.77	92.01066	0.8834449

Reboiler Heat Duty	SER	%CC	PU
141311.7	10304.672	92.99499	0.9490168
142905.4	10381.405	92.97453	0.9470678
144499.1	10452.932	93.0044	0.9452366
146092.7	10518.646	93.08824	0.9434665
147686.4	10578.843	93.22133	0.9419016
149280.1	10633.893	93.39855	0.9404824
150873.8	10684.332	93.61375	0.9391697
152467.5	10730.958	93.8589	0.9379495
154061.1	10774.705	94.12519	0.9368004
155654.8	10816.504	94.40434	0.9356898
157248.5	10857.303	94.68835	0.9345729

158842.2	10897.705	94.97222	0.9334406
160435.9	10938.101	95.25308	0.9322673
162029.6	10978.715	95.52958	0.9310474
163623.2	11019.709	95.80096	0.9297862
165216.9	11061.271	96.06622	0.9284959
166810.6	11103.599	96.3242	0.9271892
168404.3	11146.843	96.57394	0.9259133
169998	11191.089	96.8148	0.9246678

Condenser Heat Duty	SER	%CC	PU
6600.5	10433.74	96.30508	0.9488021
6822.717	10441.261	96.30522	0.953469
7044.934	10447.198	96.30509	0.9571191
7267.15	10451.854	96.30461	0.9599183
7489.367	10455.48	96.30382	0.9620517
7711.584	10458.293	96.30278	0.9636689
7933.801	10460.466	96.30158	0.964892
8156.018	10462.137	96.30031	0.9658161
8378.234	10463.418	96.29903	0.9665154
8600.451	10464.44	96.29753	0.967032
8822.668	10465.32	96.2955	0.9674278
9044.885	10466.001	96.29377	0.9677355
9267.102	10466.563	96.29212	0.9679691
9489.318	10467.001	96.29085	0.968134
9711.536	10467.337	96.28986	0.9682709
9933.753	10467.604	96.28907	0.9683743
10155.97	10467.812	96.2885	0.9684492
10378.19	10467.967	96.28814	0.968507
10600.4	10468.067	96.28804	0.9685527

Appendix B

Creating a neural network function.

```
function [net]=w_Create(net)

ms_time=str2num(datestr(now,'FFF'));
RStr = RandStream('mcg16807','Seed',ms_time);
RandStream.setGlobalStream(RStr);


M=net.M;
layers=net.layers;
inputs=net.nn(1);
delay=net.delay;


X=[];
U=[];
I=cell(M,1);


%--------------------------
dI{1,1}=delay.In;
for d=dI{1,1}
    IW{1,1,d+1}= (-0.5 + 1.*rand(layers(1),inputs));
end
X=[1];
I{1}=1;

%---------------------------------------

for m=1:M
    L_b{m}=[];
    L_f{m}=[];


    if m>1
        l=m-1;
        dL{m,l}=0;
        LW{m,l,1}=(-0.5 + 1.*rand(layers(m),layers(l)));
        L_b{l}=m;
        L_f{m}=[L_f{m},l];
    end
```

```
    for l=m:M

        if (m==1)&&(l==M)
            dL{m,l}=delay.Out;
        else
            dL{m,l}=delay.Intern;
        end

        for d=dL{m,l}
            LW{m,l,d+1}=(-0.5 + 1.*rand(layers(m),layers(l)));

            if (sum(l==L_f{m})==0)

                L_f{m}=[L_f{m},l];

            end
            if (l>=m)&&(d>0)

                if (sum(m==X)==0)

                    X=[X,m];

                end
                if (sum(l==U)==0)

                    U=[U,l];

                end
            end
        end
    end

    b{m}=(-0.5 + 1.*rand(layers(m),1));
end

if (sum(M==U)==0)
    U=[U,M];
end

for  u=U
    CX_LW{u}=[];
    for x=X
```

```
        if
(size(intersect(u,L_f{x}))>0)&(sum(x==CX_LW{u})==0)&(any(dL{x,
u}>0))
            CX_LW{u}=[CX_LW{u},x];
        end
    end
end

for x=1:M
    CU_LW{x}=[];
    for u=U
        if any(dL{x,u}>0)
            CU_LW{x}=[CU_LW{x},u];
        end
    end
end

net.U=U;
net.X=X;
net.dL=dL;
net.dI=dI;
net.L_b=L_b;
net.L_f=L_f;
net.I=I;
net.CU_LW=CU_LW;
net.CX_LW=CX_LW;

net.w_0=Wb2w(net,IW,LW,b);
```

Train RNN using LM algorithm

```
function net=train_LM(P,Y,net,k_max,E_stop)

dampconst   =     10;
dampfac    =     3;

[data,net] = prepare_data(P,Y,net);

[J,E,e]=RTRL(net,data);

k=1;
Ek(k)=E;
```

```
disp(['Iteration: ', num2str(k),'   Error: ', num2str(E),'
SkalFakt:', num2str(dampfac)])

while 1

    JJ=J'*J;
    w=net.w;

    while 1

G=(JJ+dampfac.*eye(size(JJ,1)))\eye(size(JJ+dampfac.*eye(size(
JJ,1))));

        g=J'*e;
        if isnan(G(1,1))
            w_delta=-1/1e10.*g;
        else
            w_delta=-G*g;
        end
        net.w=w+w_delta;
        [E2] = calc_error(net,data);
        if E2<E
            dampfac=dampfac/dampconst;
            break;
        elseif E2>=E
            dampfac=dampfac*dampconst;
        end
    end

    [J,E,e,a]=RTRL(net,data);
    k=k+1;
    Ek(k)=E;
    disp(['Iteration: ', num2str(k),'   Error: ', num2str(E),'
SkalFakt:', num2str(dampfac)])

    if (k>=k_max) || (E<=E_stop)
           break
    end

end

net.ErrorHistory=Ek;
```